CHAPTER 5

Hyperspectral Imaging Instruments

Jianwei Qin

US Department of Agriculture, Agricultural Research Service, Henry A. Wallace Beltsville Agricultural Research Center, Beltsville, Maryland, USA

5.1. INTRODUCTION

CONTENTS

Optical sensing technologies offer great potential for nondestructive evaluation of agricultural commodities. Approaches based on imaging and spectroscopy have been intensively investigated and developed for many years. Although they have been used in various agricultural applications, conventional imaging and spectroscopy methods have limitations to obtain sufficient information from individual food items. In recent years, hyperspectral imaging has emerged as a better solution for quality and safety inspection of food and agricultural products. A comparison for the three approaches mentioned above may help better understand the merits of the hyperspectral imaging technique. General system configurations for conventional imaging, conventional spectroscopy, and hyperspectral imaging are illustrated in Figure 5.1. A conventional imaging system mainly consists of a light source and an area detector. The light source provides illumination to the sample, and the area detector captures mixed spectral contents from the sample. Spatial information of the sample is obtained in the forms of monochromatic or colorful images. Major components in a conventional spectroscopy system include a light source, a wavelength dispersion device, and a point detector. Light is dispersed into different wavelengths after interaction with the sample, and the point detector collects the dispersed light to obtain spectral information from the sample. Due to the size limitation of the point detector, the spectroscopy measurement cannot cover large areas or small areas with high spatial resolution. Hyperspectral imaging technique combines

Hyperspectral Imaging for Food Quality Analysis and Control

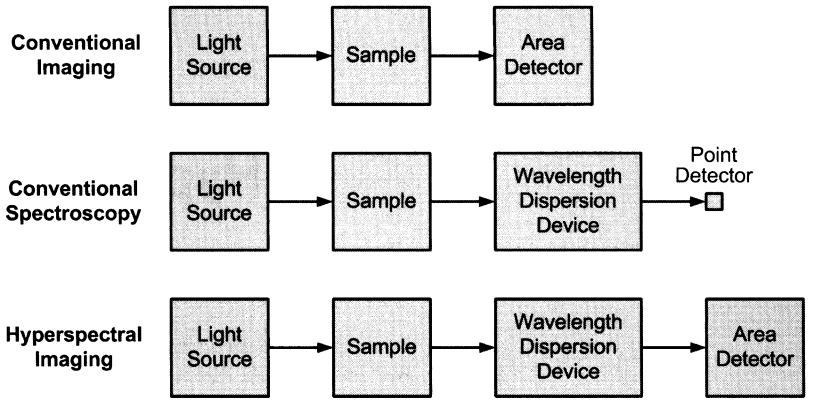

FIGURE 5.1 *General system configurations for conventional imaging, conventional spectroscopy, and hyperspectral imaging*

conventional imaging and spectroscopy techniques. A typical hyperspectral system consists of a light source, a wavelength dispersion device, and an area detector. It is capable of acquiring both spatial and spectral information from the sample in a form of spatially organized spectroscopy. If conventional imaging tries to answer the question *where* and conventional spectroscopy tries to answer the question *what*, then hyperspectral imaging tries to answer the question *where is what*.

Instrumentation is the base of any reliable measurement system. Selection of the instruments and design of their setup and calibrations are crucial for the performance of hyperspectral imaging systems. With proper arrangement, some instruments used for conventional imaging and spectroscopy can also be used for hyperspectral imaging. There are also instruments specifically designed for hyperspectral imaging. This chapter primarily focuses on instrumentation for hyperspectral imaging technique, with an emphasis on those that have found applications in food quality analysis and control. There is a brief introduction of methods for hyperspectral image acquisition (Section 5.2), with basic concepts and ground rules for the rest of the chapter. Main attention is paid to introduce a variety of essential components for constructing hyperspectral imaging systems (Section 5.3), including light sources, wavelength dispersion devices, and detectors. Instruments and methods for calibrating hyperspectral imaging systems such as spatial calibration, spectral calibration, and flat-field correction are also discussed (Section 5.4). Conclusions are given by summarizing the chapter and addressing the future development of hyperspectral imaging instruments (Section 5.5).

5.2. METHODS FOR HYPERSPECTRAL IMAGE ACQUISITION

Hyperspectral images are three-dimensional (3-D) in nature. Generally there are four approaches that can be used for acquiring 3-D hyperspectral image cubes [hypercubes (x, y, λ)]. They are point scanning, line scanning, area scanning, and the single shot method, as illustrated in Figure 5.2. In the point-scanning method (also known as the whiskbroom method), a single point is scanned along two spatial dimensions (x and y) by moving either the sample or the detector. A spectrophotometer equipped with a point detector is used to acquire a spectrum for each pixel in the scene. Hyperspectral image data are accumulated pixel by pixel in an exhaustive manner. Two-axis motorized positioning tables are usually needed to finish the image acquisition. The line-scanning method (also known as the pushbroom method)

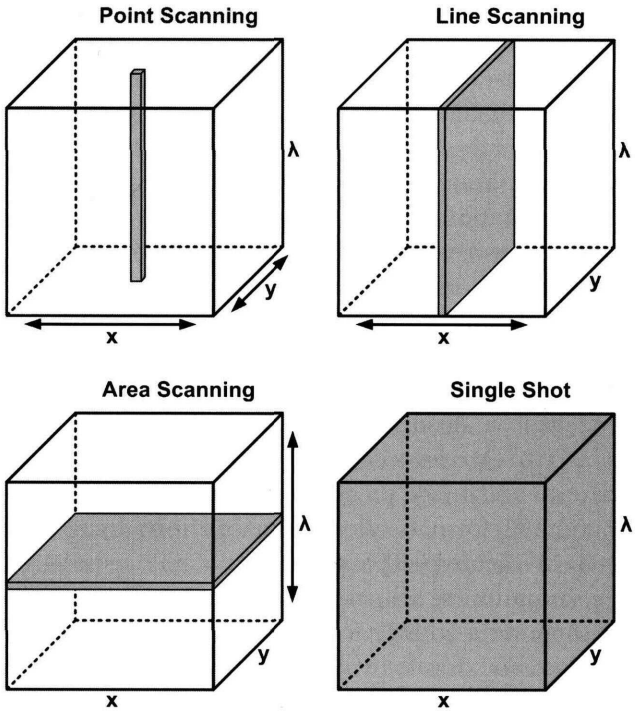

FIGURE 5.2 *Methods for acquiring three-dimensional hyperspectral image cubes containing spatial (x and y) and spectral (λ) information. Arrows represent scanning directions, and gray areas represent data acquired at a time*

can be considered as an extension of the point-scanning method. Instead of scanning one point each time, this method simultaneously acquires a slit of spatial information as well as spectral information corresponding to each spatial point in the slit. A special 2-D image (y, λ) with one spatial dimension (y) and one spectral dimension (λ) is taken at a time. A complete hypercube is obtained as the slit is scanned in the direction of motion (x). Hyperspectral systems based on imaging spectrographs with either fixed or moving slits work in the line-scanning mode.

Both point scanning and line scanning are spatial-scanning methods. The area-scanning method (also known as band sequential method), on the other hand, is a spectral-scanning method. This approach acquires a single band 2-D grayscale image (x, y) with full spatial information at once. A hypercube containing a stack of single band images is built up as the scanning is performed in the spectral domain through a number of wavelengths. No relative movement between the sample and the detector is required for this method. Imaging systems using filters (e.g., filter wheels containing fixed bandpass filters and electronically tunable filters) or Fourier transform imaging spectrometers belong to the area-scanning method. At last, the single shot method is intended to record both spatial and spectral information on an area detector with one exposure. No scanning in either spatial or spectral domains is needed for obtaining a 3-D image cube, making it attractive for applications requiring fast hyperspectral image acquisitions. This method is still in the early stage and not fully developed. Only a few implementations that rely on complicated fore-optics design and computationally intensive postprocessing for image reconstructions are currently available, with limitations for ranges and resolutions for spatial and spectral dimensions.

The 3-D hyperspectral image cubes acquired by point-scanning, line-scanning, and area-scanning methods are generally stored in the formats of Band Interleaved by Pixel (BIP), Band Interleaved by Line (BIL), and Band Sequential (BSQ), respectively. Different formats have different advantages in terms of image processing operations and interactive analysis. The BIP and BSQ formats offer optimal performances for spectral and spatial accesses of the hyperspectral image data, respectively. The BIL format gives a compromise in performance between spatial and spectral analysis. The three data storage formats can be converted to each other. The single shot method usually utilizes a large area detector to capture the images. The spatial and spectral contents from each frame can be transformed in either format mentioned above using appropriate reconstruction algorithms.

5.3. INSTRUMENTS FOR CONSTRUCTING HYPERSPECTRAL IMAGING SYSTEMS

The essential components for constructing hyperspectral imaging systems include light sources, wavelength dispersion devices, and area detectors. They are introduced in the following sections.

5.3.1. Light Sources

Light serves as an information carrier for vision-based inspection systems. Light sources generate light that illuminates or excites the target. Choice of the light sources and design of the lighting setup are critical for the performance and reliability of any imaging system. There are numerous types of light sources available for imaging or non-imaging applications. In this section, selected representative illumination and excitation light sources suitable for hyperspectral imaging applications are introduced.

5.3.1.1. Halogen lamps

Halogen lamps are the most common broadband illumination sources used in visible (VIS) and near-infrared (NIR) spectral regions. In their typical form, a lamp filament made of tungsten wire is housed in a quartz glass envelope filled with halogen gas. Light is generated through incandescent emission when a high operation temperature is on the filament. The halogen gas helps remove the deposited tungsten on the inside of the envelope and return it to the filament, maintaining the bulb is cleanliness and a long-term stable output for the lamp. The output light of quartz–tungsten–halogen (QTH) lamps forms a smooth continuous spectrum without sharp spectral peaks in the wavelength range from visible to infrared. The QTH lamps are bright light sources and are operated with low voltage, and they are the popular all-purpose illumination sources. The disadvantages of the halogen lamps include large heat generation, relatively short lifetime, output variations due to operating voltage fluctuations, spectral peak shift due to temperature change, and sensitivity to vibration.

The halogen lamps are commercially available in various forms. They can be used directly to illuminate the target (like room lighting) or be put in a lamp housing, from which light is delivered through an optical fiber. Figure 5.3 shows a DC-regulated halogen fiber-optic illuminator produced by TechniQuip (Danville, CA, USA). It generates light by a 150-watt halogen lamp inside, and offers a variable intensity control from 0 to 100%. A cold mirror is placed on the backside of the lamp to reflect the light to the fiber bundle. Coupled with proper fiber-optic light guides, the unit can deliver

FIGURE 5.3 *A halogen fiber-optic illuminator produced by TechniQuip (photo courtesy of TechniQuip, Danville, CA, USA). (Full color version available on http://www.elsevierdirect.com/companions/9780123747532/)*

broadband light for different illumination purposes (e.g., line light for hyperspectral line scanning and ring light for hyperspectral area scanning). The tungsten halogen lamps have been intensively used as light sources in hyperspectral reflectance measurements for surface inspections (Kim *et al.*, 2001; Lu, 2003; Park *et al.*, 2002). High intensity lamps have also been used in hyperspectral transmittance measurements for detecting inside agricultural commodities (Ariana & Lu, 2008; Qin & Lu, 2005; Yoon *et al.*, 2008).

5.3.1.2. Light emitting diodes

Owing to the demand for cheap, powerful, robust, and reliable light sources, light emitting diode (LED) technology has advanced rapidly during the past few years. Unlike tungsten halogen lamps, LEDs do not have a filament for incandescent emission. Instead, they are solid state sources that emit light when electricity is applied to a semiconductor. They can generate narrowband light in the VIS region at different wavelengths (or colors), depending on the materials used for the p–n junction inside the LED. Recently, LEDs that can produce high intensity broadband white light have been developed (Steigerwald *et al.*, 2002). Currently there are two major approaches to generate white light with LEDs. One approach mixes red, blue, and green monochromatic lights from three independent LEDs to generate the white light (Muthu *et al.*, 2002). The other approach utilizes a blue LED to excite a phosphor coating to form a phosphor-converted LED

(pcLED) (Mueller-Mach *et al.*, 2002). The phosphor converts partial energy of the blue light into red and green light. The white light is created by mixing the generated red and green light with the rest of the blue light. This is the commonly used approach at present. Figure 5.4(a) shows a spectrum emitted by a white LED using the pcLED approach. It has a fairly good output in the VIS region. A spectral peak can be observed in the blue region around 470 nm due to the leaked blue light.

A picture of a LED line light produced by Advanced Illumination (Rochester, VT, USA) is shown in Figure 5.4(b). It is a high intensity source that can provide white light for long working distance or large area imaging

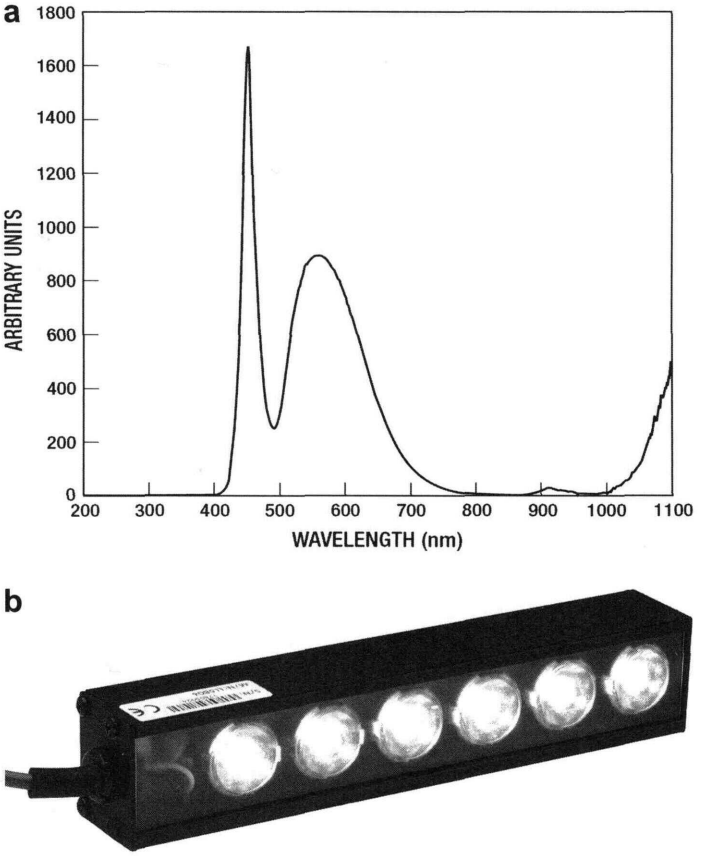

FIGURE 5.4 *Light emitting diode (LED): (a) emission spectrum of a white LED (courtesy of Newport Corporation, Irvine, CA, USA) and (b) a LED line light produced by Advanced Illumination (photo courtesy of Advanced Illumination, Inc., Rochester, VT, USA). (Full color version available on http://www.elsevierdirect.com/companions/9780123747532/)*

applications. Its operating temperature is below 60 °C, and the lamp lifetime is 50 000 hours, which is at least one order higher than that of most tungsten halogen lamps. As a new type of light source, LEDs have a lot of advantages over traditional lighting, such as long lifetime, low power consumption, low heat generation, small size, fast response, robustness, and insensitivity to vibration. They can be assembled in different arrangements (e.g., spot, line, and ring lights) to satisfy different illumination requirements. The LED technology is still ongoing with the development of new materials and electronics. LEDs have great potential to become mainstream light sources beyond their traditional uses such as small indicator lights on instrument panels. With the various benefits mentioned above, LED lights have started to find uses in the area of food quality and safety inspection (Chao *et al.*, 2007; Lawrence *et al.*, 2007). The use of LEDs as new light sources for hyperspectral imaging applications is likely to expand in the near future.

5.3.1.3. Lasers

Tungsten halogen lamps and white LEDs are illumination sources that are generally used in hyperspectral reflectance and transmittance imaging applications. The spectral constitution of the incident broadband light is not changed after light-sample interactions. The measurement is performed based on intensity changes at different wavelengths. Unlike broadband illumination sources, lasers are powerful directional monochromatic light sources. Light from lasers is generated through stimulated emission, which typically occurs inside a resonant optical cavity filled with a gain medium, such as gas, dye solution, semiconductor, and crystal. They can operate in CW (continuous wave) mode or pulse mode in terms of temporal continuity of the output. Lasers are widely used as excitation sources for fluorescence and Raman measurements owing to their unique features such as highly concentrated energy, perfect directionality, and real monochromatic emission.

Excited by a monochromatic light with a high energy, some biological materials (e.g., animal and plant tissues) emit light of a lower energy in a broad wavelength range. The energy change (or frequency shift) can cause fluorescence emission or Raman scattering that carries composition information of the target. Both fluorescence imaging and Raman imaging are sensitive optical techniques that can detect subtle changes of biological materials. Lasers have found applications in hyperspectral fluorescence imaging for inspection of agricultural commodities. For example, Kim *et al.* (2003) used a 355 nm pulsed Nd:YAG laser as an excitation source to perform fluorescence measurement for contaminant detection of apple and

pork samples. Noh & Lu (2007) applied a 408 nm CW blue diode laser on apples to excite chlorophyll fluorescence. The hyperspectral laser-induced fluorescence images were analyzed for evaluating apple fruit quality. Lasers have also been utilized as excitation sources in hyperspectral Raman imaging applications (Jestel *et al.*, 1998; Wabuyele *et al.*, 2005). Besides lasers, other types of sources such as high-pressure arc lamps (e.g., xenon), low-pressure metal vapor lamps (e.g., mercury), and ultraviolet (UV) fluorescent lamps can also serve as excitation sources. In addition, LEDs that can produce narrowband pulsed or continuous light have started to be used as excitation sources, although at present their output has lower intensities and broader bandwidths than lasers.

5.3.1.4. Tunable sources

The configuration shown in Figure 5.1 is adopted by most current hyperspectral imaging systems for food quality and safety inspection. That is, the wavelength dispersion device is positioned between the sample and the detector. Light is dispersed into different wavelengths after interaction with the sample. There is another equivalent approach that puts the wavelength dispersion device in the illumination light path instead of the imaging light path (Figure 5.5a). This approach can be used by the hyperspectral systems that rely on broadband illumination (e.g., reflectance and transmittance imaging). Combined with the wavelength dispersion device, the white light source becomes a tunable light source. Incident light is dispersed before reaching the sample. There is no difference in principle between the two approaches for hyperspectral measurements. The major advantage of the tunable source approach is that the wavelength dispersion device does not need to maintain the spatial information of the target (Klein *et al.*, 2008). The detector directly performs area scanning to obtain both spatial and spectral information from the sample. The wavelength dispersion device should be synchronized with the detector to achieve automatic image acquisition. The intensity of the illumination using tunable sources is relatively weak since only narrowband light is incident on the sample at a time.

Tunable light sources are still in an early stage of development. Various wavelength dispersion methods have the potential to be adopted for making the tunable sources. Figure 5.5(b) shows an example of tunable source based on an acousto–optic tunable filter (AOTF) produced by Brimrose (Sparks, MD, USA). Its major components include a white light source and an AOTF device and its driver. Narrowband light is generated at a time when the white light interacts with the AOTF device. The source operates in the wavelength range of 360–560 nm with a spectral resolution up to 1 nm. To

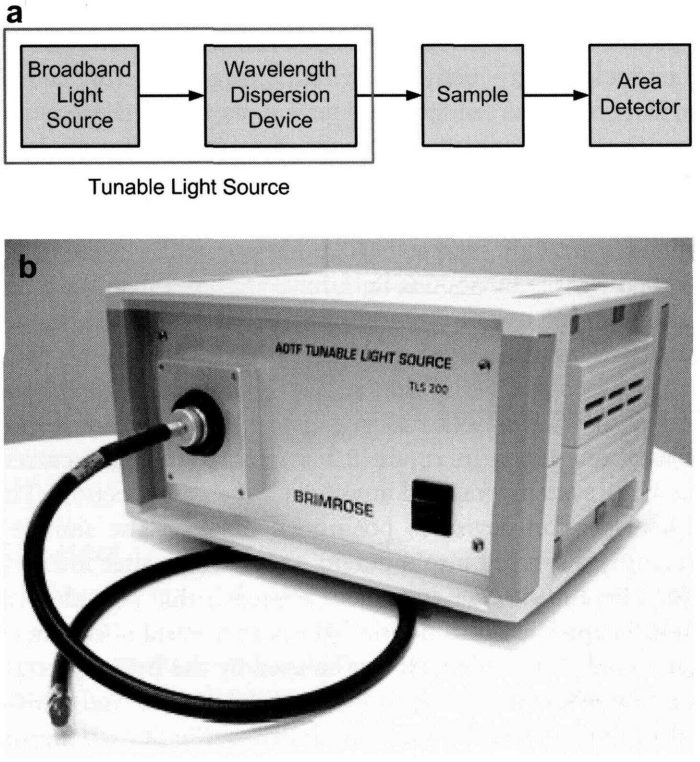

FIGURE 5.5 *Tunable light source: (a) concept and (b) a tunable light source based on acousto-optic tunable filter (AOTF) produced by Brimrose (photo courtesy of Brimrose Corporation, Sparks, MD, USA). (Full color version available on http://www.elsevierdirect.com/companions/9780123747532/)*

date, the use of tunable light sources for hyperspectral imaging applications is still limited because of the immature development of the related hardware. Efforts have been made to apply the tunable sources to hyperspectral reflectance and transmittance imaging, especially for the measurement conditions where weak illumination is desired to protect the target (e.g., document analysis and verification). Brauns & Dyer (2006) used a Michelson interferometer in front of a tungsten source to provide illumination for document samples at different wavelengths. Hyperspectral transmittance images were acquired for identification of fraudulent documents. Klein *et al.* (2008) put discrete bandpass filters between a broadband source and the target to fulfill a tunable light source. Hyperspectral reflectance measurement was performed for analyzing historical documents. Details on the operating principles of the wavelength dispersion devices mentioned above (i.e., AOTF, Michelson interferometer, and bandpass filter) can be found in

Section 5.3.2. The introduction of tunable sources opens a new avenue for implementation of hyperspectral image acquisition. Their feasibility for agricultural applications needs to be explored.

5.3.2. Wavelength Dispersion Devices

Wavelength dispersion devices are the heart of any hyperspectral imaging system. Various optical and electro–optical instruments can be used in hyperspectral imaging systems for dispersing broadband light into different wavelengths. The commonly used wavelength dispersion devices as well as some newly developed instruments are presented in this section. Their advantages and disadvantages for hyperspectral imaging applications are also discussed.

5.3.2.1. Imaging spectrographs

An imaging spectrograph is an optical device that is capable of dispersing incident broadband light into different wavelengths instantaneously for different spatial regions from a target surface. It can be considered as an enhanced version of the traditional spectrograph in that the imaging spectrograph can carry spatial information in addition to the spectral information. The imaging spectrograph generally operates in line-scanning mode, and it is the core component for the pushbroom hyperspectral imaging systems. Most contemporary imaging spectrographs are built based on diffraction gratings. A diffraction grating is a collection of transmitting or reflecting elements separated by a distance comparable to the wavelength of the light under investigation. The fundamental physical characteristic of the diffraction grating is the spatial modulation of the refractive index, by which the incident electromagnetic wave has its amplitude and/or phase modified in a predictable manner (Palmer, 2005). There are two main approaches in constructing imaging spectrographs, and they are transmission gratings (i.e., a grating laid on a transparent surface) and reflection gratings (i.e., a grating laid on a reflective surface).

Figure 5.6(a) illustrates the general configuration of an imaging spectrograph utilizing a transmission grating. Specifically, the operating principle of this imaging spectrograph is based on a prism–grating–prism (PGP) construction. An incoming light from the entrance slit of the spectrograph is collimated by the front lens. The collimated beam is dispersed at the PGP component so that the direction of the light propagation depends on its wavelength. The central wavelength passes symmetrically through the prisms and grating and stays at the optical axis. The shorter and longer

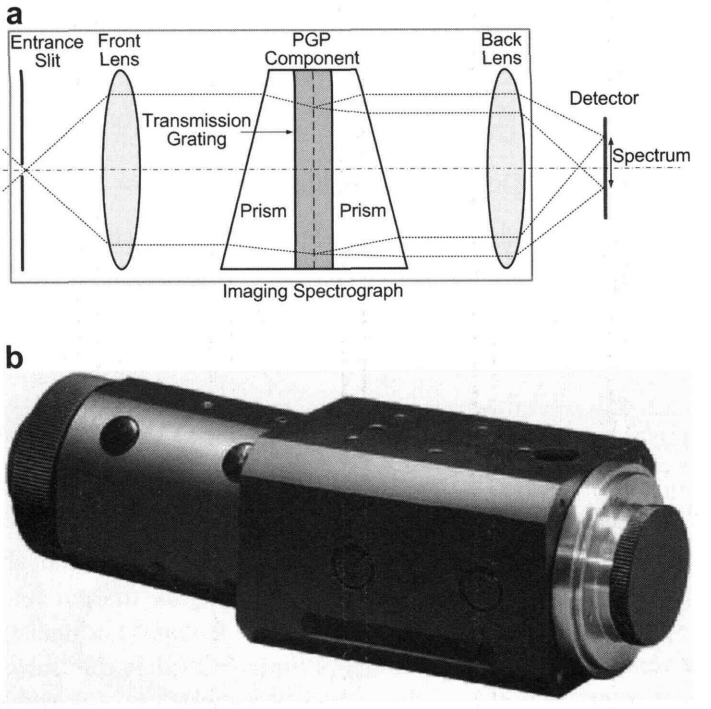

FIGURE 5.6 *Prism–grating–prism (PGP) imaging spectrograph: (a) operating principle and (b) an ImSpector imaging spectrograph produced by Spectral Imaging Ltd. (photo courtesy of Spectral Imaging Ltd., Oulu, Finland). (Full color version available on http://www.elsevierdirect.com/companions/9780123747532/)*

wavelengths are dispersed up and down relative to the central wavelength. This design results in a minimum deviation from the ideal on-axis condition and minimizes geometrical aberrations in both spatial and spectral axes (Spectral Imaging, 2003). As a result, the light from the scanning line is dispersed into different wavelengths, and they are projected onto an area detector through the back lens, creating a special two-dimensional image: one dimension represents spatial information and the other dimension spectral. As shown in Figure 5.6(a), each vertical line along the spectral axis of the 2-D area detector forms a continuous spectrum from a fixed spatial point of the object surface.

Figure 5.6(b) shows a commercialized PGP-based imaging spectrograph (ImSpector series) produced by Spectral Imaging Ltd. (Oulu, Finland). The ImSpector series includes several versions of imaging spectrographs covering different wavelength ranges e.g., UV (200–400 nm), VIS (380–780 nm),

and NIR (900–1700 nm). Besides the standard series, enhanced and fast versions of the ImSpectors are also available to meet the requirements of high spectral and spatial resolutions as well as high speed spectral image acquisitions. The one shown in Figure 5.6(b), for example, is an ImSpector V10E imaging spectrograph. It is designed for the VIS and short-wavelength NIR region. The spectral range covered by this imaging spectrograph is 400–1000 nm. The slit length is 14.2 mm, and the spectral resolution under the default silt width (30 μm) is 2.8 nm. The slit width is customizable to realize different spectral resolutions. The ImSpectors have the merits of small size, ease of mounting, and common straight optical axis. They can be easily attached to a lens and a monochrome area detector to form a line-scanning spectral camera system. For the past decade, the ImSpector imaging spectrographs have been widely used throughout the world in standard or customized forms for developing many hyperspectral imaging systems. The ImSpector-based measurement systems have been applied for analyzing physical and/or chemical properties of a broad range of food and agricultural products. Examples include detecting contaminants on apples (Kim *et al.*, 2001) and poultry carcasses (Park *et al.*, 2002), tumors on chicken skin (Chao *et al.*, 2002), bruises on apples (Lu, 2003), pits in tart cherries (Qin & Lu, 2005), internal defects in cucumbers (Ariana & Lu, 2008), canker lesions on citrus (Qin *et al.*, 2008), and cracks in the shell of eggs (Lawrence *et al.*, 2008).

Reflection gratings are intensively used for making various conventional monochromators and spectrographs. Depending on the surface geometry of the diffraction gratings, plane gratings and curved gratings (i.e., concave and convex) are two basic types of the reflection gratings that are used in practice. Many optical layouts exist for constructing different types of monochromators and spectrographs. Examples include Czerny–Turner, Ebert–Fastie, Monk–Gillieson, Littrow, Rowland, Wadsworth, and flat-field configurations (Palmer, 2005). Reflection gratings have recently been used to build imaging spectrographs. For example, Headwall Photonics (Fitchburg, MA, USA) developed hyperspectral imaging spectrographs (Hyperspec series, Figure 5.7b) based on the Offner configuration (Figure 5.7a). The unit is constructed entirely from reflective optics. The basic structure of the design involves a pair of concentric spherical mirrors coupled with an aberration-corrected convex reflection grating. As shown in Figure 5.7(a), the lower mirror is used to guide the incoming light from the entrance slit to the reflection grating, where the incident beam is dispersed into different wavelengths in a reflection manner. The upper mirror then reflects the dispersed light to the detector, where a continuous spectrum is formed. This configuration offers the advantage of high image quality, free of

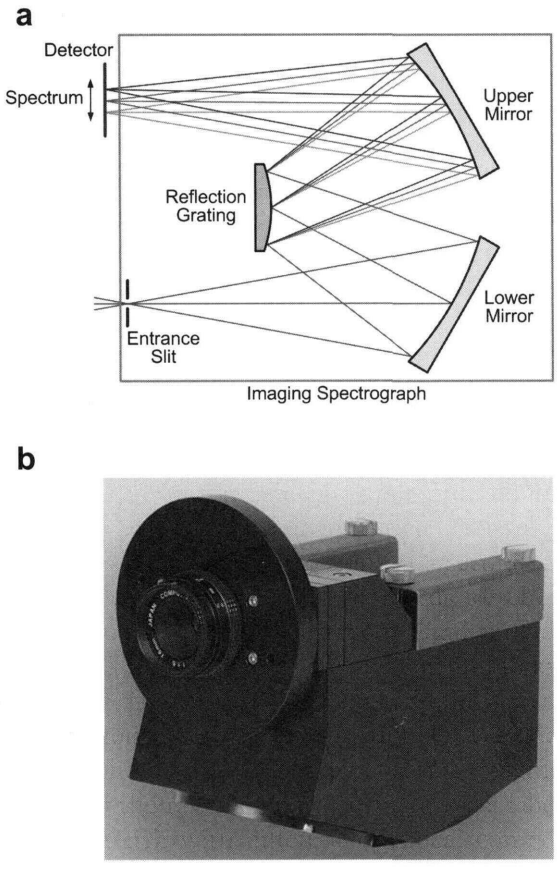

FIGURE 5.7 *Offner imaging spectrograph: (a) operating principle and (b) a Hyperspec imaging spectrograph produced by Headwall Photonics (photo courtesy of Headwall Photonics, Fitchburg, MA, USA). (Full color version available on http://www.elsevierdirect.com/companions/9780123747532/)*

higher-order aberrations, low distortion, low f-number, and large field size (Bannon & Thomas, 2005). The reflection gratings are not limited by the transmission properties of the grating substrate. Additionally, the reflective optical components (e.g., mirrors) generally have higher efficiencies than the transmission components (e.g., prisms). Thus the reflection grating-based imaging spectrographs are ideal for the situations where high signal-to-noise ratio (SNR) is crucial for measurement. The imaging spectrograph utilizing the reflection grating approach represents an increasingly accepted instrument for line-scanning hyperspectral imaging systems, especially for the low light measuring conditions such as fluorescence imaging and Raman imaging.

5.3.2.2. Filter wheels

The most basic implementation of spectral imaging is the use of a rotatable disk called a filter wheel carrying a set of discrete bandpass filters (Figure 5.8b). The main characteristic of the bandpass filters is that they transmit a particular wavelength with high efficiency while rejecting light energy out of the passband (Figure 5.8a). As the filter wheel employs mechanical rotation, the light perpendicularly transmits across different filters, generating a series of narrow band images at different predetermined wavelengths. Interference filters are commonly used as optical bandpass filters. Modern interference filters are constructed with a series of thin films (usually a few nanometers thick) between two glass plates. Each film layer is made from a dielectric material with a specified refractive index. The incident light to the filter is affected by interferences due to different refractive indices of the films. High

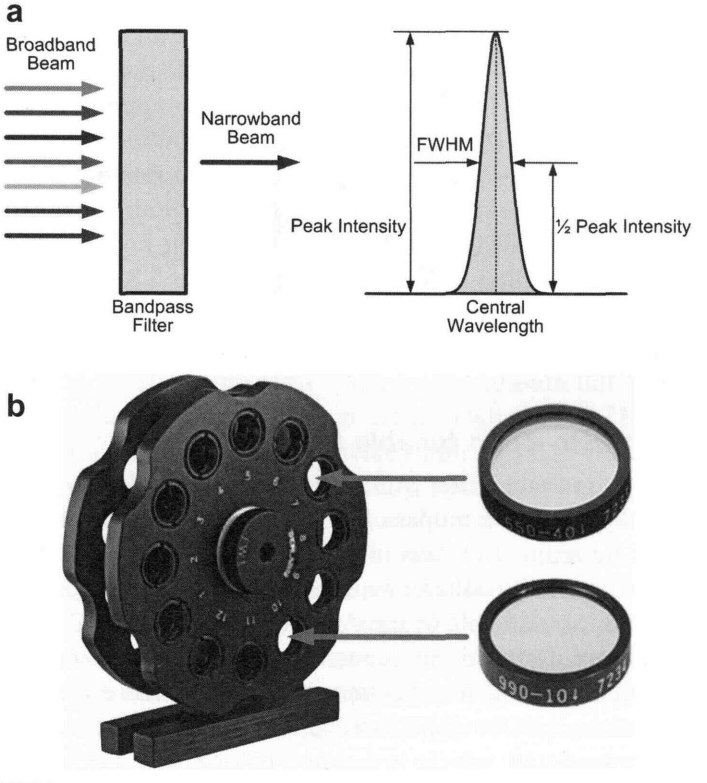

FIGURE 5.8 *Optical bandpass filter: (a) concept and (b) filter wheel and interference bandpass filters (photo courtesy of Thorlabs, Newton, NJ, USA). (Full color version available on http://www.elsevierdirect.com/companions/9780123747532/)*

reflectance will occur for the wavelengths undergoing destructive interferences, whereas high transmittance will occur for other wavelengths undergoing constructive interferences. The interference bandpass filters are generally designed for collimated light that is normally incident on the filter surface. The light with incident angles other than normal will cause an undesired output such as shift of the central wavelength and change of the transmission region. Large incident angles will cause a significant decrease for the transmittance of the passband.

Central wavelength (i.e., wavelength corresponding to peak transmission) and spectral bandwidth that is defined as full width at half maximum (FWHM) (Figure 5.8a) are two key parameters for the bandpass filters. A broad range of filters with various specifications are commercially available to meet the requirements of different applications. Different mechanical configurations of the filter wheels (e.g., single-wheel and dual-wheel) can hold different numbers of filters. Beside manual control, filter wheels that are electronically controlled are also available. They can be synchronized with the camera system to fulfill automatic filter switching and image acquisition. The filter wheels are easy to use and relatively inexpensive. However, they have some limitations for hyperspectral imaging applications, such as narrow spectral range and low resolution, slow wavelength switching, mechanical vibration from moving parts, and image misregistration due to the filter movement. The spectral range and the resolution are determined by the number and the bandwidth of the filters that can be housed in the wheels. The one with double filter holders shown in Figure 5.8(b) can carry up to 24 filters. If the filters with 10 nm FWHM are used, the wavelength range covered by the filter wheel system is 240 nm.

5.3.2.3. Acousto–optic tunable filters

An acousto–optic tunable filter (AOTF) is a solid state device that works as an electronically tunable bandpass filter based on light–sound interactions in a crystal. The major function of the AOTF is to isolate a single wavelength of light from a broadband source in response to an applied acoustic field. The operating principle of the AOTF is illustrated in Figure 5.9(a). It mainly consists of a crystal, an acoustic transducer, an acoustic absorber, a variable source working at radio frequencies (RF), and a beam stop. The most common crystal for constructing the AOTF is Tellurium Dioxide (TeO_2). The transducer, which is bonded to one side of the crystal and controlled by the RF source, generates high frequency acoustic waves through the crystal. The acoustic waves change the refractive index of the crystal by compressing and relaxing the crystal lattice. The variations of

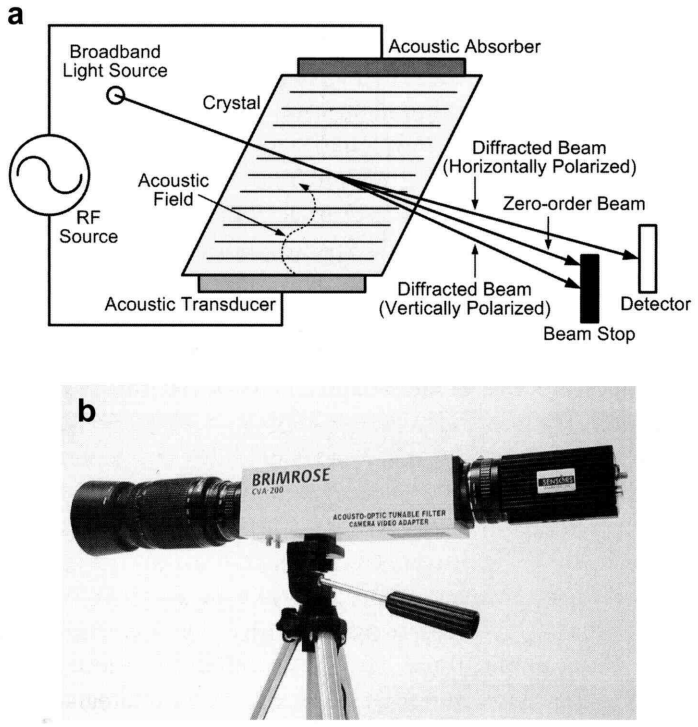

FIGURE 5.9 *Acousto—optic tunable filter (AOTF): (a) operating principle and (b) an AOTF camera video adapter produced by Brimrose (photo courtesy of Brimrose Corporation, Sparks, MD, USA). (Full color version available on http://www.elsevierdirect.com/companions/9780123747532/)*

the refractive index make the crystal like a transmission diffraction grating. The incident light is diffracted after going through the AOTF. As shown in Figure 5.9(a), the diffracted light is divided into two first-order beams with orthogonal polarizations (i.e., horizontally polarized and vertically polarized). Both diffracted beams can be used in certain applications. The undiffracted zero-order beam and the undesired diffracted beam (e.g., vertically polarized beam in Figure 5.9a) are blocked by the beam stop. Similar to a bandpass filter with a narrow bandwidth, the AOTF only diffracts light at one particular wavelength at a time. The wavelength of the isolated light is a function of the frequency of the acoustic waves that are applied to the crystal. Therefore, the wavelength of the transmitted light can be controlled by varying the frequency of the RF source. Wavelength switching for the AOTF is very fast (typically in tens of microseconds) owing to the fact that the tuning speed is only limited by the speed of the sound propagation in the crystal. In addition to the wavelength separation, the

bandwidth and the intensity of the filtered light can also be adjusted through the control of the RF source.

Important features of the AOTF include high optical throughput, moderate spectral resolution, broad spectral range, fast wavelength switching, accessibility of random wavelength, and flexible controllability and programmability (Morris *et al.*, 1994). The AOTFs have the ability to transmit single-point signals and 2-D images in the VIS and NIR spectral regions. They can be used to build spectrophotometers as well as hyperspectral imaging systems. Figure 5.9(b) shows a commercial AOTF camera video adapter produced by Brimrose (Sparks, MD, USA). The adapter is designed for acquiring hyperspectral images in the VIS and NIR spectral regions. The aperture size of the adapter is 10×10 mm. It is available in three wavelength ranges (i.e., 400–650 nm, 550–1000 nm, and 900–1700 nm) by using different AOTF devices. The corresponding spectral resolutions are in the range of 2 to 20 nm. A zoom lens and a CCD (charge-coupled device) camera are mounted at the front and back ends of the AOTF adapter, respectively. The AOTF hyperspectral imaging system provides narrow bandwidth, fast wavelength selection, and intensity control of the output light. The AOTF-based hyperspectral imaging systems have been used in agricultural applications, such as estimation of leaf nitrogen and chlorophyll concentrations (Inoue & Penuelas, 2001) and detection of green apples in the field (Safren *et al.*, 2007).

5.3.2.4. Liquid crystal tunable filters

A liquid crystal tunable filter (LCTF) is a solid state instrument that utilizes electronically controlled liquid crystal cells to transmit light with a specific wavelength with the elimination of all other wavelengths. The LCTF is constructed from a series of optical stacks, each consisting of a combination of a birefringent retarder and a liquid crystal layer inserted between two parallel polarizers. A single filter stage including the essential optical components is shown in Figure 5.10(a). The incident light is linearly polarized through the polarizer. It is then separated into two rays (i.e., ordinary and extraordinary) by the fixed retarder. The ordinary and the extraordinary rays have different optical paths through the retarder, and they emerge with a phase delay that is dependent upon the wavelength of the light. The polarizer behind the retarder only transmits those wavelengths of light in phase to the next filter stage. Each stage transmits the light as a sinusoidal function of the wavelength, with the frequency determined by the thickness of the retarder and the difference of the refractive index between the ordinary and the extraordinary rays at the wavelength of the light. The transmitted light adds constructively in the desired passband and destructively in the

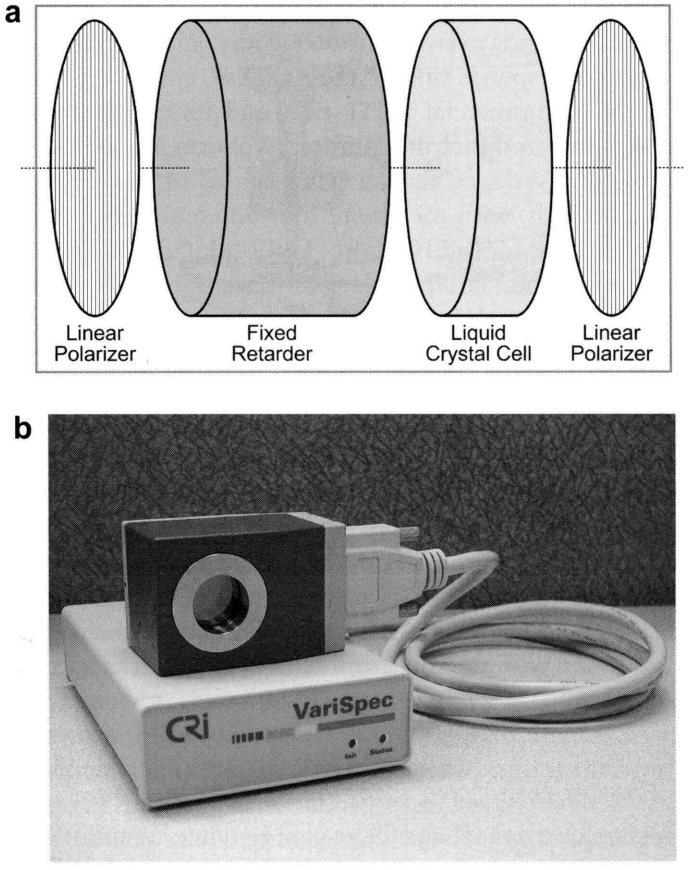

FIGURE 5.10 *Liquid crystal tunable filter (LCTF): (a) single filter stage and (b) a VariSpec LCTF and its controller produced by Cambridge Research and Instrumentation (CRi) (photo courtesy of Cri, Inc., Woburn, MA, USA). (Full color version available on http://www.elsevierdirect.com/companions/9780123747532/)*

other spectral regions. All the individual filter stages are connected in series, and they function together to transmit a single narrow band. A liquid crystal cell is used in each filter stage to realize electronic tunability. An electric field is applied between the two polarizers which causes small retardance changes to the liquid crystal layer. The electronic controller of the LCTF is able to shift the narrow passband region throughout the entire wavelength range covered by the filter unit. A single LCTF unit generally covers a specific wavelength range because the components for constructing the filter have different characteristics that can only accommodate a particular spectral region. The wavelength switching speed depends on the relaxation time of

the liquid crystal as well as the number of stages in the filter. Typically, it takes tens of milliseconds to switch from one wavelength to another, which is far longer than the response time of the AOTFs.

A picture of a commercial LCTF unit and its controller produced by Cambridge Research and Instrumentation (Woburn, MA, USA) is shown in Figure 5.10(b). The VariSpec series LCTFs can cover the VIS to NIR range from 400 to 2450 nm, with the use of four different LCTF units [i.e., VIS (400–720 nm), SNIR (650–1100 nm), LNIR (850–1800 nm), and XNIR (1200–2450 nm)]. The VariSpec devices have relatively large apertures (20–35 mm), and the bandwidths of the filters are in the range of 7–20 nm, making them suitable for imaging and non-imaging applications requiring moderate spectral resolutions. The LCTF approach for hyperspectral imaging has found a number of applications in the research of food quality and safety inspection, such as estimation of apple fruit firmness (Peng & Lu, 2006), fungal detection in wheat (Zhang *et al.*, 2007), and early inspection of rottenness on citrus (Gómez-Sanchis *et al.*, 2008a). Compared to the fixed interference filters used in the filter wheels, the electronically tunable filters including AOTFs and LCTFs can be flexibly controlled through the computer. Also, they do not have moving parts and therefore do not suffer the problems associated with the rotating filter wheels, such as speed limitation, mechanical vibration, and image misregistration.

5.3.2.5. Fourier transform imaging spectrometers

Self interference of a broadband light can generate an interferogram that carries its spectral information. An inverse Fourier transform to the generated interferogram can reveal the constitution of the frequencies (or wavelengths) of the broadband light. That is the fundamental principle of Fourier transform interference spectroscopy. The simplest form of the two-beam interferometers is the Michelson interferometer, which is widely used in commercial Fourier transform spectrometers working in the infrared region. It consists of a beamsplitter and two flat mirrors (fixed mirror and moving mirror) that are perpendicular each other (Figure 5.11a). Light from the source is divided into two beams at a beamsplitter that has a semi-reflecting coating on the surface. The light is partially reflected to the fixed mirror, and the remaining energy is transmitted through the beamsplitter to the moving mirror, which moves in a parallel direction with the incident light. The beams reflected back from the two mirrors are recombined by the same beamsplitter. The moving mirror introduces optical path difference (OPD) between the two beams. Interferograms are then generated and collected by the detector.

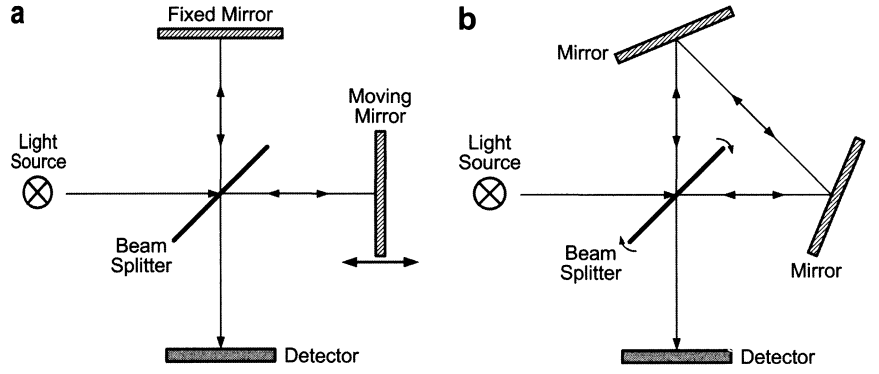

FIGURE 5.11 *Principles of interferometers: (a) Michelson interferometer and (b) Sagnac interferometer*

Different from the Michelson interferometer, the Sagnac interferometer is a common-path two-beam interferometer. The major components of the Sagnac interferometer include two fixed mirrors arranged in a specified angle and a beamsplitter that can be slightly rotated (Figure 5.11b). Two separated beams from the beamsplitter travel the same path in opposite directions. They are recombined at the beamsplitter after traversing the triangular loops. The OPD between the two beams is a function of the angular position of the beamsplitter. Interference fringes can be created by tuning the beamsplitter at very small angles. Hyperspectral images can be acquired by rotating the beamsplitter in a stepwise manner. An interferogram is generated for each spatial point on the sample surface. The spectral information is obtained by Fourier analysis of the interferograms. Although most interferometers are susceptible to vibrations, especially for light with short wavelengths, the Sagnac interferometers are stable and easy to align owing to the fact that they rely on the beamsplitter's rotation other than the mirror's translation to generate interference patterns (Hariharan, 2007). This advantage extends the working range of the traditional Fourier transform interference spectroscopy from the infrared to the visible and short-wavelength near-infrared regions. The wavelength dispersion devices based on Fourier transform techniques have the advantages of high optical throughput, high spectral resolution, and flexible selection of the wavelength range. Varying sensitivity in the entire spectral region and intense computation for data transform are two shortcomings for practical applications.

Applied Spectral Imaging (Vista, CA, USA) developed hyperspectral imaging systems (SpectraCube series) based on the rotating Sagnac interferometer (Malik *et al.*, 1996). Several settings can be adjusted depending on

the field of view, spatial resolution, spectral region and resolution, and signal-to-noise ratio. Spectral resolution is uneven across the whole wavelength range. Shorter wavelengths have higher resolutions than longer wavelengths. Image acquisition speed is moderate. According to Pham *et al.* (2000), it takes 40 s to acquire a hyperspectral image cube with a dimension of 170 × 170 × 24 (24 bands) covering the spectral region of 550–850 nm. SpectraCube imaging systems have been used in biomedical research, such as examination of human skin lesions (Orenstein *et al.*, 1998), quantification of absorption and scattering properties of turbid materials (Pham *et al.*, 2000), and spectral karyotyping for prenatal diagnostics (Mergenthaler-Gatfield *et al.*, 2008).

5.3.2.6. Single shot imagers

One example of single shot hyperspectral imagers is the computed tomography imaging spectrometer (CTIS), which can be considered as an application of computed tomography (CT) in imaging spectrometry (Descour & Dereniak, 1995; Okamoto & Yamaguchi, 1991). In this method, multiplexed spatial and spectral data are collected simultaneously to fulfill the acquisition of a complete hyperspectral image cube using one exposure of an area detector. Implementation of a CTIS generally involves a computer-generated hologram (CGH) disperser, a large 2-D area detector, and other optical components for light collimation and image formation (Descour *et al.*, 1997). The CGH element is the central component of the CTIS, and its function is to disperse the field of view into multiple diffraction orders. The dispersed images form a mosaic on the large area detector. Each subimage is not a single band image, but the result of both spectral and spatial multiplexing. The spectral information of the original scene is encoded in the positions and intensities of the subimages in the mosaic. Reconstruction algorithms similar to those used in tomographic imaging techniques are utilized to rebuild the 3-D hypercubes from the original 2-D image data.

More recently, Bodkin Design and Engineering (Wellesley Hills, MA, USA) developed a hyperspectral imager with the capacity to acquire a hypercube in one snapshot (Figure 5.12). The design is based on the company's so called HyperPixel Array technology (Bodkin, 2007). The imaging system includes two stages for optical signal processing. A 2-D lenslet array or a 2-D pinhole array is used to resample an image from the fore-optics (i.e., the first stage) of the imager. The field of view is divided into multiple spatial channels. Each channel is then dispersed into multiple spectral signatures, and they are collected by a 2-D focal plane array. The detector can obtain spectral content of all the pixels (so called HyperPixels) in

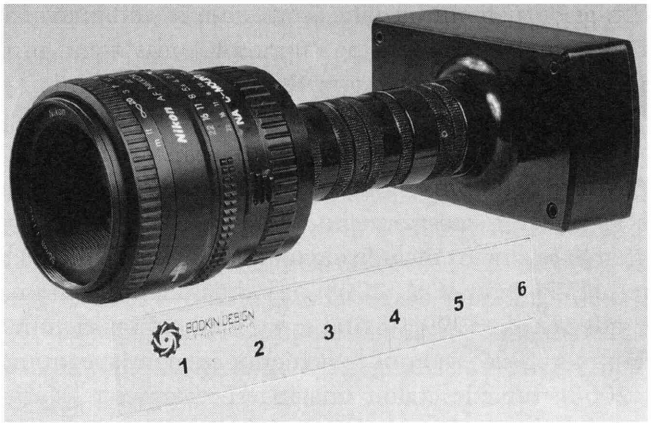

FIGURE 5.12 *A single shot hyperspectral imager produced by Bodkin Design and Engineering (photo courtesy of Bodkin Design and Engineering, Wellesley Hills, MA, USA). (Full color version available on http://www.elsevierdirect.com/companions/9780123747532/)*

real time. Generation of the hypercubes purely relies on the parallel optical signal processing performed in the second stage, making it not dependent on computations for image reconstructions. Details for the optical system design of the Bodkin hyperspectral imagers can be found in Bodkin *et al.* (2008). The one shown in Figure 5.12 (VNIR-20) is able to capture hyperspectral images with a dimension of 100 × 180 × 20 (20 bands) at a speed of 20 cubes/s. It works in the VIS range (425–675 nm) with a low spectral resolution (12.5 nm/pixel on average). Another model (VNIR-90) works in the spectral region of 490–925 nm with a higher spectral resolution (3.9 nm/pixel on average). The spatial resolution of this imager is relatively low, and it can acquire hyperspectral images with a dimension of 55 × 44 × 90 (90 bands) at a speed of 15 cubes/s.

The major advantage of single shot hyperspectral imagers is their speed for capturing 3-D images. The line-scanning and area-scanning methods are time-consuming for building hypercubes. It is difficult to perform hyperspectral image acquisitions for fast-moving samples using scanning imagers. The single shot systems can obtain all the spatial and spectral data from a sample at video frame rates, making it possible to generate a hypercube in tens of milliseconds. This feature is especially useful for real-time hyperspectral imaging applications, such as on-line quality and safety inspection of food and agricultural products. The current single shot imagers can work in a broad wavelength range with high spectral resolution at a cost of scarifying spatial resolution. Improvements are needed to address the issue of low spatial resolution, which could limit their applications for circumstances

requiring high-resolution spatial data. Single shot devices that can capture 3-D hypercubes without any scanning represent a new trend in instrument development for hyperspectral imaging techniques.

5.3.2.7. Other instruments

Besides the wavelength dispersion devices described above, there are also other types of imaging spectrometers that can be used in hyperspectral imaging systems. Examples include circular variable filters (CVF) and linear variable filters (LVF) (Min *et al.*, 2008), Hadamard transform imaging spectrometer (Hanley *et al.*, 1999), digital array scanned interferometer (DASI) (Smith & Hammer, 1996), volume holographic imaging spectrometer (VHIS) (Liu *et al.*, 2004), tunable etalon imaging spectrometer (Marinelli *et al.*, 1999), etc. Details for the operating principles of these designs are omitted for brevity, and they can be found in the literature provided. Wavelength dispersion instruments are the core of hyperspectral imaging systems. New technologies are being introduced to create new devices in this area. For example, a new type of electronically tunable filter has recently been developed based on microelectromechanical systems (MEMS) technology (Abbaspour-Tamijani *et al.*, 2003; Goldsmith *et al.*, 1999). Such filters are constructed using MEMS variable capacitors, and they have similar functions with AOTFs and LCTFs. Owing to their merits such as extremely small size and low power consumption, the MEMS-based tunable filters have the potential to be used to build miniature hyperspectral imaging systems (e.g., hand-held instruments). Meanwhile, current instruments can also be modified or improved to satisfy specific requirements of different applications. For example, moving slit design can be introduced to imaging spectrographs so that line scanning can be performed with both sample and detector remaining stationary (Lawrence *et al.*, 2003). Introduction of new design concepts and improvement of current instruments are main drivers for the future development of hyperspectral imaging technology.

5.3.3. Area Detectors

After interacting with the target and going through the wavelength dispersion device, light carrying the useful information will eventually be acquired by a detector. The function of the detector is to measure the intensity of the collected light by converting radiation energy into electrical signals. The performance of the detector directly determines the quality of the images. Two major types of solid state area detectors including CCD (charge-coupled device) and CMOS (complementary metal-oxide-semiconductor) cameras are introduced in this section.

5.3.3.1. CCD cameras

The CCD sensor is composed of many (usually millions) small photodiodes (called pixels) that are made of light sensitive materials such as silicon (Si) or indium gallium arsenide (InGaAs). Each photodiode acts like an individual spot detector that converts incident photons to electrons, generating an electrical signal that is proportional to total light exposure. All the electrical signals are shifted out of the detector in a predefined manner and then are digitalized to form the images. The pixels in the CCD sensor can be arranged in one-dimensional or two-dimensional arrays, resulting in line detector and area detector, respectively. Hyperspectral imaging systems usually use area detectors to obtain the image data. Thus emphasis is put on the introduction to the CCD area detectors.

Generally there are four types of CCD architectures that are used for reading out the data from the area sensors, and they are full frame, frame transfer, interline transfer, and frame interline transfer (Figure 5.13). The full

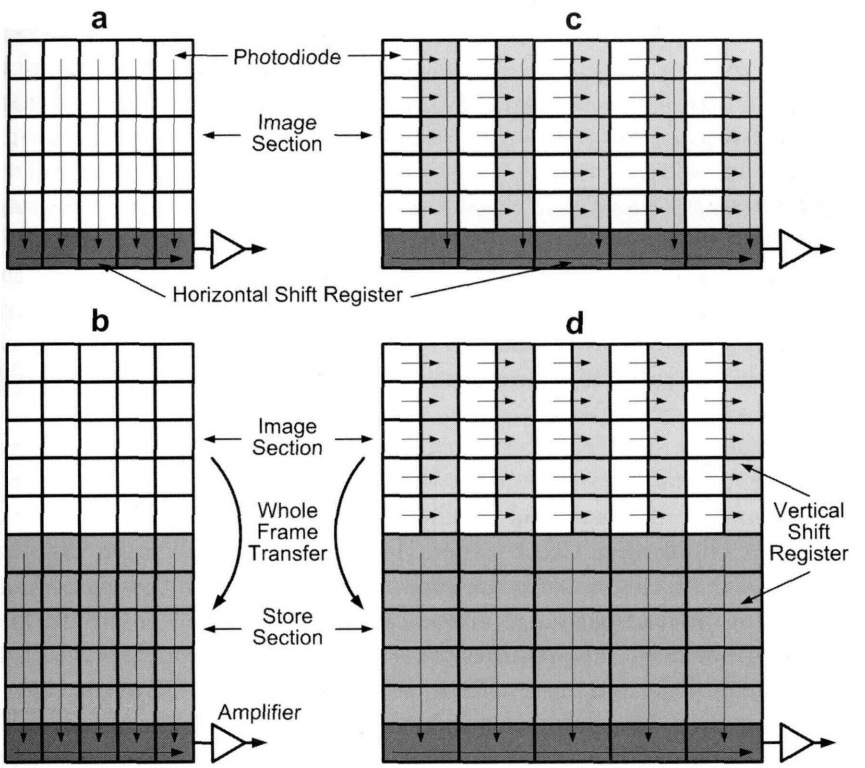

FIGURE 5.13 *Typical CCD architectures for different data transfer methods: (a) full frame; (b) frame transfer; (c) interline transfer; and (d) frame interline transfer*

frame structure is the simplest form for constructing the CCD. Electric charges are accumulated in the photosensitive section (image section) during the light integration period. Then they are vertically shifted row by row into a horizontal shift register, where each row is exported to form an array of pixels (known as a progressive scan). A mechanical shutter is usually used to cover the sensor during the process of data transfer to avoid interference of newly generated charges, making this CCD architecture relatively slow for image acquisition. The frame transfer approach extends the full frame structure by adding a new store section (normally with identical size of the image section) that is covered by a mask all the time. Accumulated charges from the image section are rapidly transferred to the store section for each whole frame. While the next light signal is integrated in the image section, the charges in the store section are shifted vertically into the horizontal register. This structure has faster frame rates than the full frame structure, at a cost of larger size of the image sensor. The interline structure, on the other hand, transfers the charge from each pixel into a corresponding vertical shift register (called interline mask), which is immediately adjacent to each photodiode and shielded from the incident light. The subsequent process is the same with the frame transfer structure. This structure is also quick at shifting the data. A disadvantage of this approach is that the interline mask on the sensor decreases the effective area for collecting the light signal. Lastly, the frame interline transfer is a combination of the frame transfer and the interline transfer. Charges in the interline mask are transferred to the store section as a whole frame, which further accelerates the data shift speed. However, it bears the disadvantages of high cost for the large sensor and reduced sensitive area. The architectures of full frame and frame transfer are adopted by most scientific cameras for quantitative measurement applications, while the two architectures using interline transfer are commonly used in various video cameras.

Many factors (e.g., sensor size, pixel size, dynamic range, readout speed, dark noise, readout noise, spectral response, cooling method, image output form, computer interface, and synchronization option) need to be considered when choosing a CCD camera for a specific application. Spectral response of the CCD sensor is an important characteristic that determines the working wavelength range of the camera. A measure of this feature, quantum efficiency (QE) quantifies the relationship between the wavelength of the incident light and the sensitivity of the camera. The QE of the CCD is primarily governed by the substrate materials used to make the photodiodes. Owing to its natural sensitivity to visible light, silicon is intensively used as sensor material for the CCD cameras working in the VIS and short-wavelength NIR regions. The spectral response of the silicon image sensors is

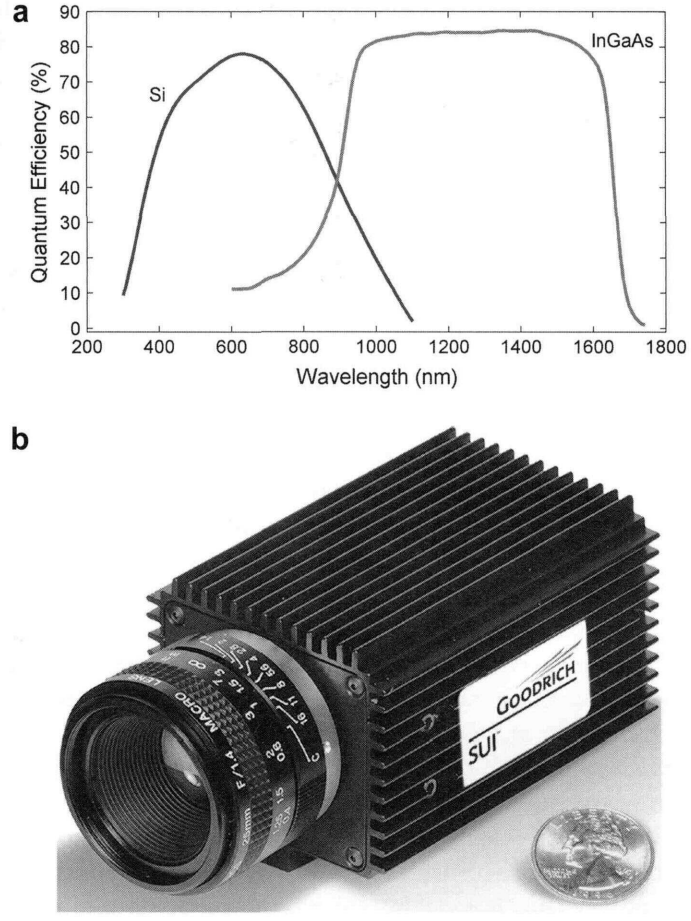

FIGURE 5.14 *Indium gallium arsenide (InGaAs) image sensor: (a) typical quantum efficiencies of silicon (Si) and InGaAs image sensors and (b) an InGaAs camera produced by Sensors Unlimited (data and photo courtesy of Sensors Unlimited, Inc., Princeton, NJ, USA). (Full color version available on http://www.elsevierdirect.com/companions/9780123747532/)*

a bell-shaped curve with QE values declined towards both UV and NIR regions (Figure 5.14a). The silicon-based CCD cameras have been widely used in hyperspectral reflectance and transmittance imaging systems for inspection of agricultural commodities using spectral information in the VIS and short-wavelength NIR regions (Kim *et al.*, 2001; Park *et al.*, 2002; Qin & Lu, 2005).

The NIR spectral region also carries plenty of useful information for food quality and safety inspection. The InGaAs image sensor, which is made of an

alloy of indium arsenide (InAs) and gallium arsenide (GaAs), has fairly flat and high quantum efficiency in the NIR region (Figure 5.14a). Standard InGaAs (53% InAs and 47% GaAs) image sensors cover the wavelength range of 900–1700 nm. Extended wavelength range (e.g., 1100–2200 nm and 1100–2600 nm) can be achieved by changing the percentages of InAs and GaAs for making the InGaAs sensors (Sensors Unlimited, 2006). In terms of quantum efficiency, the InGaAs camera starts from where the silicon camera declines, making the InGaAs camera a good choice for hyperspectral imaging systems working in the NIR region for agricultural applications (Lu, 2003; Nicolai *et al.*, 2006; Zhang *et al.*, 2007). The InGaAs camera produced by Sensors Unlimited (Princeton, NJ, USA) is shown in Figure 5.14(b). It utilizes a standard InGaAs image sensor with a sensitivity range from 900 to 1700 nm. The QE of the camera is greater than 65% in the wavelength range of 1000–1600 nm. It can work at room temperature and the frame rate is up to 60 Hz. Detectors for the mid-infrared region are also available, such as lead selenide (PbSe), indium antimonide (InSb), and mercury cadmium telluride (MCT).

The CCD camera can deliver high quality images when there is sufficient light reaching the image sensor and no short exposure is required, which is a typical condition for hyperspectral reflectance and transmittance measurements. However, for low light applications such as fluorescence imaging and Raman imaging, the regular CCD camera may not be able to obtain the data that satisfy the application requirements. High performance cameras such as Electron Multiplying CCD (EMCCD) and Intensified CCD (ICCD) cameras are usually used to acquire the images with high signal-to-noise ratio. EMCCD is a quantitative digital camera technology that is capable of detecting single photon events whilst maintaining high quantum efficiency (Andor, 2006). An EMCCD differs from a traditional CCD by adding a unique solid state electron multiplication register to the end of the normal readout register (Figure 5.15a). This built-in multiplication register multiplies the weak charge signals before any readout noise is imposed by the output amplifier, achieving real gain for the useful signals. Figure 5.15(b) shows an EMCCD camera (iXon series) produced by Andor (South Windsor, CT, USA). The electron multiplier gain of this camera can be adjusted in the range of 1–1000 through the camera software control. When there is plenty of light, the gain function can also be switched off to change the EMCCD camera to a conventional CCD camera. EMCCD cameras have started to find their applications for inspection of food and agricultural products. Kim *et al.* (2007) developed an EMCCD-based hyperspectral system to perform both reflectance and fluorescence measurements for on-line defect and fecal

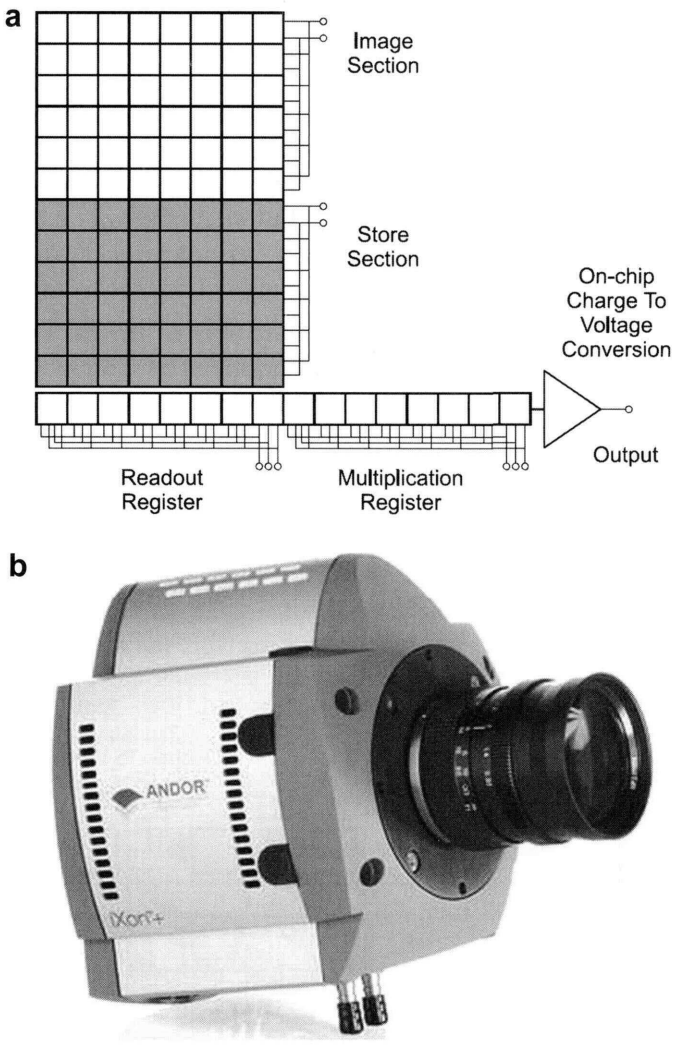

FIGURE 5.15 *Electron Multiplying CCD (EMCCD): (a) architecture and (b) an EMCCD camera produced by Andor (illustration and photo courtesy of Andor Technology PLC, South Windsor, CT, USA). (Full color version available on http://www.elsevierdirect.com/companions/9780123747532/)*

contamination detection of apples. ICCD is another type of high performance image sensor that can detect weak optical signals. Instead of adding a multiplication register after photon to electron conversion (EMCCD's approach), the ICCD utilizes an image intensifier tube to apply the gain to the incident light before it reaches the image sensor. The amplified light

signals are then coupled to the CCD. Hence the EMCCD is based on electronic amplification, while the ICCD is based on optical amplification. Besides the gain function, ICCD cameras have another important feature of being able to realize very fast gate times (in nanoseconds or picoseconds). This feature makes them suitable for detecting time-resolved signals with very short duration, such as time-dependent fluorescence emissions induced by pulsed lasers (Kim *et al.*, 2003).

5.3.3.2. CMOS cameras

Currently CCD cameras are the dominant devices in the area of image acquisition, especially for technical applications. The CMOS image sensor is another major type of solid state area detector that has the potential to compete with CCD. The major difference between these two types of detectors is that the CMOS image sensor includes both photodetector and readout amplifier in each pixel (called active pixel) (Litwiller, 2005). A typical architecture of the CMOS image sensor is shown in Figure 5.16. A photodiode is still used to sense the incident light, as it does in the CCD. After the photon to electron conversion, a set of optically insensitive transistors adjacent to the photodiode will convert the integrated charge to

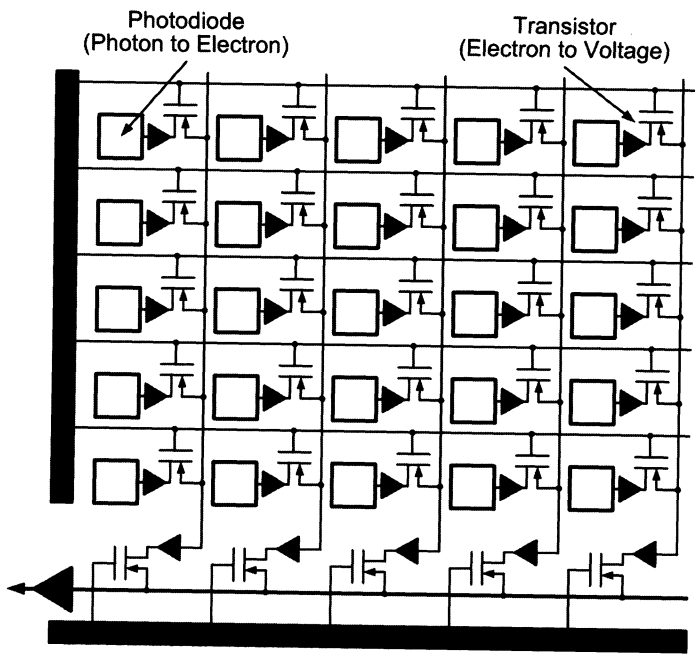

FIGURE 5.16 *Architecture of the CMOS image sensor*

a voltage signal immediately. The electron to voltage conversion occurs inside each pixel, and the generated voltage signals are then read out over the wires. Compared to the vertical and horizontal registers used by the CCD to shift the charges (see Figure 5.13), the wires used in the CMOS image sensor are much faster for signal transfer, making the CMOS cameras especially suitable for high speed imaging applications such as on-line industrial inspection. Owing to the addressability of the wires arranged in rows and columns, it is possible to extract a region of interest (ROI) from the sensor rather than the whole image, which can be utilized for on-chip image manipulations (e.g., zoom and pan). Besides the features of high speed and random addressing, the CMOS cameras have other advantages such as low cost, low power consumption, single power supply, and small size for system integration, which makes them prevail in the consumer electronics market (e.g., low-end camcorders and cell phones). The main reason that limits their applications in quantitative measurements is that the current CMOS image sensors have higher noise and higher dark current than the CCDs due to the on-chip circuits used for signal amplification and transfer. Consequently the dynamic range and the sensitivity are lower than those of CCDs. Hyperspectral imaging systems generally have higher requirements for cameras than conventional imaging systems since they also need to acquire spectral information. The CMOS cameras still need substantial performance improvement to challenge the CCD cameras in hyperspectral imaging as well as other scientific applications.

5.4. INSTRUMENTS FOR CALIBRATING HYPERSPECTRAL IMAGING SYSTEMS

Before proper measurements can be achieved, appropriate calibrations for hyperspectral imaging systems are needed. The commonly used calibration methods and instruments are introduced in the following sections.

5.4.1. Spatial Calibration

Spatial calibration for hyperspectral imaging systems is intended to determine the range and the resolution for the spatial information contained in the hypercubes. The calibration results are useful for adjusting the field of view and estimating the spatial detection limit. Different spatial calibration methods can be used for the imaging systems utilizing different image acquisition modes. The hyperspectral systems working in the area-scanning

mode generate a series of single band images at different wavelengths. Each single band image is a regular 2-D grayscale image with full spatial information. Hence the spatial calibration can be performed at a selected wavelength using printed targets with square grids or standard test charts such as US Air Force 1951 test chart. The area-scanning systems generally have the same resolution for both spatial dimensions if the same binning is used for the horizontal and vertical axis of the camera. For the line-scanning imaging systems, the resolution for the two spatial dimensions could be different. The x direction is for the stepwise movement of the samples (see Figure 5.2), and the resolution depends on the step size of the movement. The y direction is parallel to the slit of the imaging spectrograph, and the resolution is determined by the combination of the working distance, lens, imaging spectrograph, and camera.

An example of spatial calibration for a line-scanning hyperspectral imaging system is shown in Figure 5.17. The system is developed based on an imaging spectrograph (ImSpector V10, Spectral Imaging Ltd., Oulu, Finland), and it works in line-scanning mode to collect hyperspectral reflectance images from fruit and vegetable samples carried by a precision motor-controlled stage (Qin & Lu, 2008). The step size of the stage used for image acquisition is 1.0 mm. Thus the spatial resolution for the x direction (see Figure 5.2) of the hypercubes is 1.0 mm/pixel. The spatial range for the

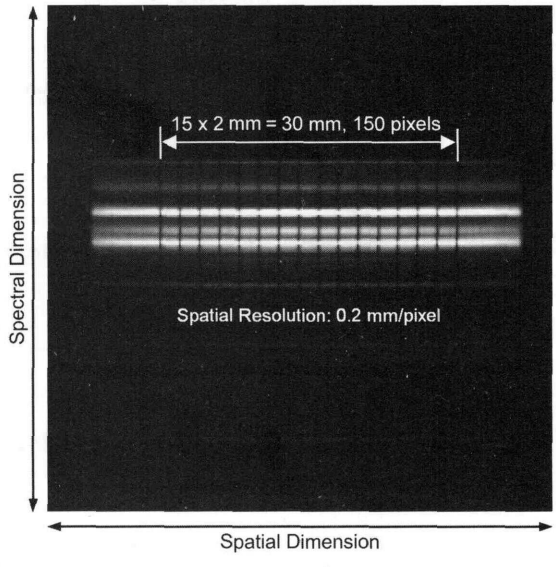

FIGURE 5.17 *Spatial calibration for a line-scanning hyperspectral imaging system using a white paper printed with thin parallel lines 2 mm apart*

x direction is determined by the number of scans. The spatial axis of the imaging spectrograph is aligned to the horizontal dimension of the CCD detector. Thus the horizontal dimension of the line-scanning images represents spatial information and the vertical dimension spectral. The one shown in Figure 5.17 is a line-scanning image with a dimension of 256 × 256. It is obtained from a white paper printed with thin parallel lines 2 mm apart, which is illuminated by a fluorescent lamp. The spatial resolution for the y direction (see Figure 5.2) of the hypercubes can be determined by dividing the real spatial distance by the number of image pixels in this range. Specifically, there are 150 pixels within 30 mm spatial distance (15 intervals with 2 mm apart for adjacent lines), thus the spatial resolution for the y direction can be calculated as 30 mm/150 pixels = 0.2 mm/pixel. The spatial range for the y direction covered by the imaging system is 0.2 mm/pixel × 256 pixels = 51.2 mm.

5.4.2. Spectral Calibration

Spectral calibration for hyperspectral imaging systems is intended to define the wavelengths for the pixels along the spectral dimension of the hypercubes. The calibration results can be used for determining the range and the resolution for the spectral information contained in the hypercubes. The area-scanning systems using fixed or tunable filters can generate single band images at a series of known wavelengths. Therefore the spectral calibration is usually not necessary. The central wavelengths of the interference bandpass filters housed in the filter wheel are generally used as the wavelengths for the corresponding single band images. The wavelengths through the tunable filters (e.g., AOTFs and LCTFs) are determined by their electronic controllers. On the other hand, imaging spectrograph-based line-scanning systems generate hypercubes with unknown wavelengths. Hence spectral calibration is needed to map the pixel indices along the spectral dimension to the exact wavelengths. The calibration can be performed utilizing spectrally well-known light sources, such as spectral calibration lamps, lasers (e.g., 632.8 nm by helium–neon [HeNe] lasers), fluorescent lamps, and broadband lamps equipped with interference bandpass filters. Spectral calibration lamps are the most commonly used calibration sources. They generate narrow, intense spectral lines from the excitation of various rare gases and metal vapors. Because a given chemical element only emits radiation at specific wavelengths, the wavelengths produced by the calibration lamps are considered to be absolute, and they are used as standards for spectral calibration. Various calibration lamps are available for the wavelength range from UV to NIR. Choices include lamps

FIGURE 5.18 *A pencil style spectral calibration lamp and its power supply produced by Newport (photo courtesy of Newport Corporation, Irvine, CA, USA)*

using argon, krypton, neon, xenon, mercury, mercury–argon, mercury–neon, mercury–xenon, etc. Such calibration lamps are commercially available for use under different circumstances (e.g., pencil style lamps, battery powered lamps, and high power lamps). Figure 5.18 shows a pencil style spectral calibration lamp and its power supply produced by Newport (Irvine, CA, USA).

An example of spectral calibration for a line-scanning hyperspectral imaging system is illustrated in Figure 5.19. The imaging system is the same as that used for demonstration of spatial calibration (Figure 5.17). Details for the hyperspectral system can be found in (Qin & Lu, 2008). The spectral calibration is performed using two pencil style spectral calibration lamps (i.e., a xenon lamp [model 6033] and a mercury–argon lamp [model 6035], Newport, Irvine, CA, USA), which have several good peaks in the wavelength range of 400–1000 nm. Two images on the top are original line-scanning images from xenon and mercury–argon lamps. Two spectral profiles are extracted along the vertical axis (spectral dimension) of the line-scanning images. The spectral peaks from each lamp and their corresponding pixel positions in the vertical axis are identified. The relationship between the vertical pixel indices and the known wavelengths from the two lamps is established using a linear regression function. The resulting linear model then can be used to determine all the wavelengths along the spectral dimension. Nonlinear regression models are also used for the spectral calibration (Chao *et al.*, 2007; Park *et al.*, 2002). Nominal spectral resolution of the imaging spectrograph is linearly dependent on the slit width (Spectral Imaging, 2003). The spectrograph used in this calibration (ImSpector V10, Spectral Imaging Ltd., Oulu, Finland) has a 25 μm slit width, and its nominal resolution is 3 nm. The calculated spectral resolution

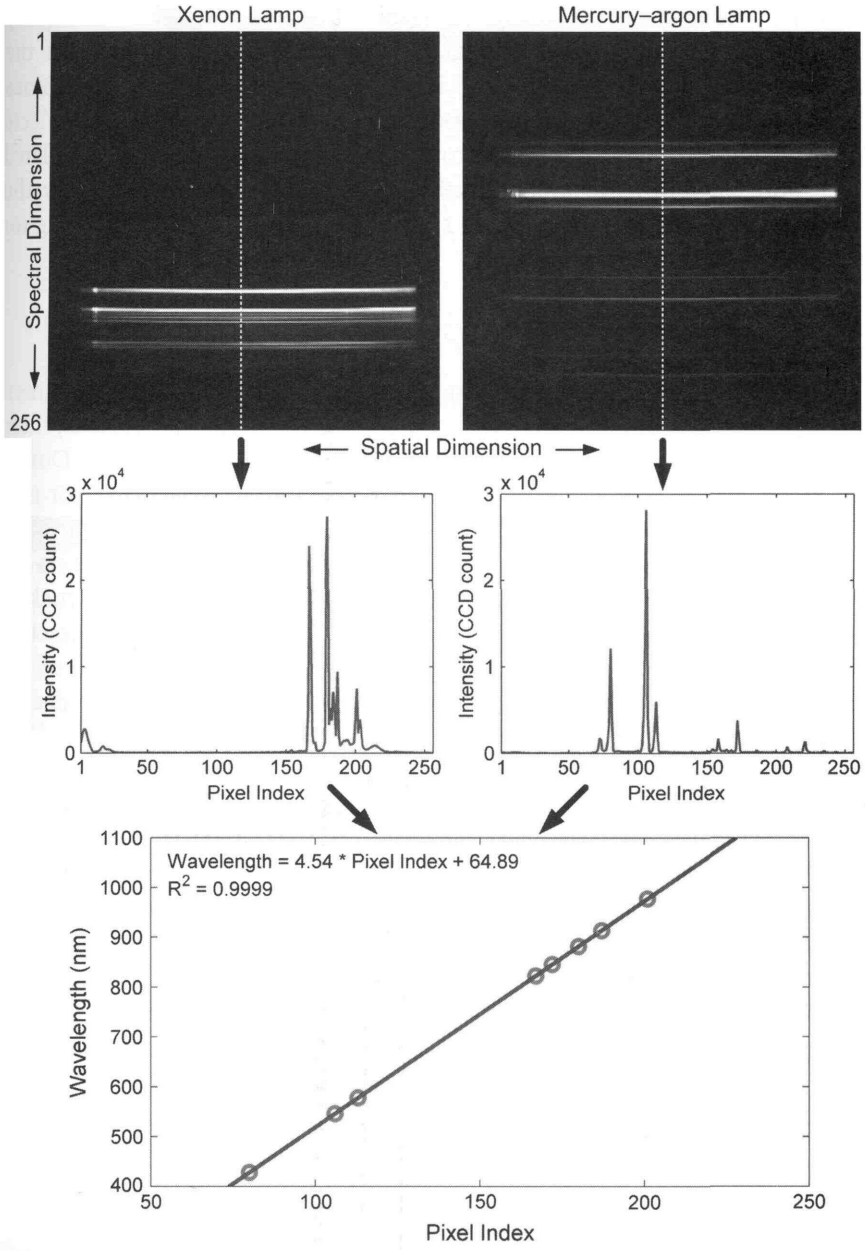

FIGURE 5.19 *Spectral calibration for a line–scanning hyperspectral imaging system using xenon and mercury–argon calibration lamps. (Full color version available on http://www.elsevierdirect.com/companions/9780123747532/)*

from the linear model shown in Figure 5.19 is 4.54 nm, which is slightly lower than the one of the spectrograph. It should be noted that it is the nominal spectral resolution of the imaging spectrograph that determines the accuracies for the spectral measurements. The camera merely collects dispersed light signals passing through the spectrograph. The calculated resolution based on the image pixel measurements is determined by the nominal resolution of the imaging spectrograph as well as the binning for the vertical axis of the detector.

5.4.3. Flat-field Correction

Raw hyperspectral images contain noises and artifacts due to measurement environments and imperfections of each component (e.g., source, lens, filter, spectrograph, and camera) in the optical path of the imaging system. During the image acquisition, the noise counts accumulated on the detector may increase the pixel values beyond the true intensities. Various image artifacts can be generated by factors such as nonuniform illumination, dust on the lens surface, and pixel-to-pixel sensitivity variations of the detector, making the original images unsuitable for quantitative analysis. Flat-field correction is intended to remove the effects of the noises and artifacts. The resulting relative (or percent) reflectance instead of the absolute intensity data is usually used for further data analysis.

White diffuse reflectance panels (Figure 5.20), which have high and flat reflectance over a broad wavelength range (e.g., 250–2500 nm), are usually used as standards for the flat-field correction for hyperspectral reflectance measurement. The flat-field correction can be performed using the following equation:

$$Rs(\lambda) = \frac{Is(\lambda) - Id(\lambda)}{Ir(\lambda) - Id(\lambda)} \times Rr(\lambda) \tag{5.1}$$

where Rs is the relative reflectance image of the sample, Is is the intensity image of the sample, Ir is the reference image obtained from the white panel, Id is the dark current image acquired with the light source off and the lens covered, Rr is the reflectance factor of the white panel, and λ is the wavelength. All the variables in Equation 5.1 are wavelength dependent, and corrections should be conducted for all the wavelengths covered by the imaging system. A constant reflectance factor (Rr) of 100% can be used for simplification, although the actual reflectance values of the white panel are slightly lower and they also have small variations over a certain spectral region. Since most samples have lower reflectance than the white panel, the relative reflectance values obtained by Equation 5.1 are in the

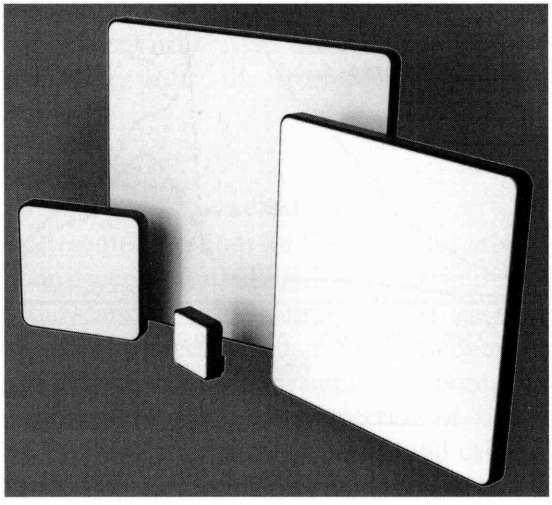

FIGURE 5.20 *White diffuse reflectance panels that can be used for flat-field corrections (photo courtesy of Labsphere, Inc., North Sutton, NH, USA)*

range of 0–100%. They can be multiplied by a constant factor (e.g., 10 000) to have a large dynamic data range and to reduce rounding errors for further data analysis.

Figure 5.21 shows an example of flat-field correction for hyperspectral reflectance measurement of a leaf sample. The plots shown in Figure 5.21(a) are original reflectance spectra extracted from three hypercubes (i.e., leaf sample, white panel [Spectralon SRT-99-100, Labsphere Inc., North Sutton, NH, USA], and dark current). Ideally, the reflectance profile of the white panel should be flat. However, the measured spectrum is bell shaped with a peak around 700 nm due to the combined spectral response of the imaging system. The white panel has the highest reflectance, and the values of the dark current are relatively low and flat over the entire wavelength range. The reflectance intensities of the leaf sample are in between. After the flat-field correction using Equation 5.1, a relative reflectance spectrum of the leaf sample is obtained (Figure 5.21b). Light absorption due to chlorophyll in the leaf can be observed around 670 nm.

5.4.4. Other Calibrations

Besides the common calibration methods described above, there are also other types of calibrations that can be performed for hyperspectral imaging systems to satisfy different measurement requirements. For example,

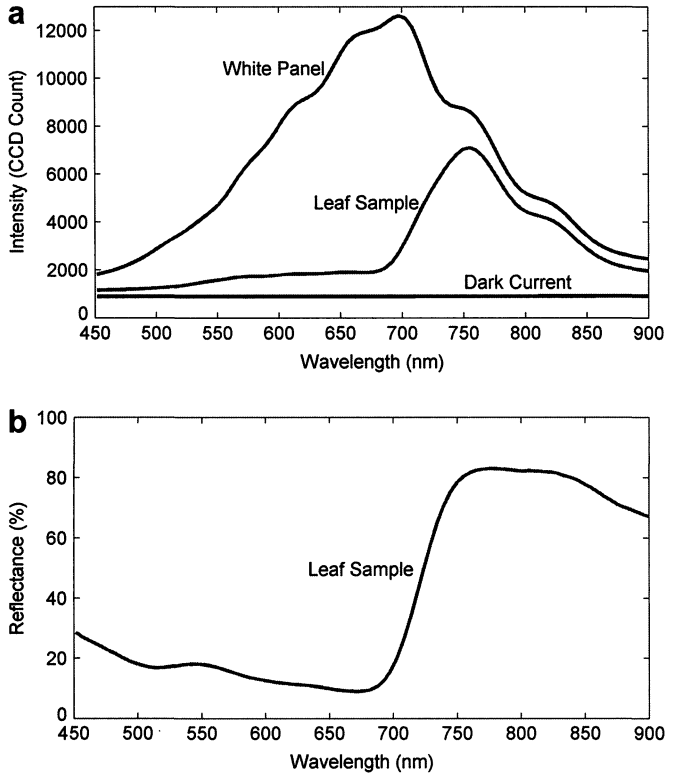

FIGURE 5.21 *Flat-field correction for hyperspectral reflectance measurement: (a) original reflectance spectra and (b) relative reflectance spectrum after flat-field correction. (Full color version available on http://www.elsevierdirect.com/companions/9780123747532/)*

radiometric calibration is required when the absolute spectral radiance of the sample is to be determined. An integrating sphere typically serves as a radiance standard for the radiometric calibration. Particular agricultural applications utilizing hyperspectral imaging can also generate particular calibration needs. For example, hyperspectral reflectance measurements for spherical fruit can not be successfully corrected by the flat-field correction due to the curvature effects. To tackle this problem, Qin & Lu (2008) developed a method for correcting spatial profiles extracted from line-scanning images of apple samples using an imaging spectrograph-based hyperspectral system. Gómez-Sanchis *et al.* (2008b) also developed a method for correcting area-scanning images from citrus samples using a LCTF-based hyperspectral system. Efforts have been made to develop various elaborate calibration methods and procedures (Burger and Geladi, 2005; Lu & Chen

1998; Lawrence *et al.*, 2003; Polder *et al.*, 2003; Qin & Lu, 2007). New effective and efficient calibration and correction approaches are expected in the future to better utilize the hyperspectral imaging techniques.

5.5. CONCLUSIONS

This chapter has presented methods for hyperspectral image acquisition and instruments for constructing and calibrating hyperspectral imaging systems. Point scanning, line scanning, area scanning, and single shot are four major methods for acquiring hyperspectral images. Various line-scanning and area-scanning hyperspectral measurement systems have been developed and used successfully for the quality and safety inspection of food and agricultural products. Related instruments for constructing and calibrating such scanning imaging systems, such as light sources, wavelength dispersion devices, detectors, standard test charts, calibration sources, and standard reflectance panels, are already commercially available. Single shot hyperspectral imagers can capture 3-D hypercubes at high speed without any scanning. They represent a new direction in hyperspectral instrument development, while such devices are still in the early development stage. New instrument design concepts will be continuously introduced, and current instruments and systems can also be improved to achieve better performance. The advances in hyperspectral imaging instruments along with the progress in hyperspectral image processing techniques will inspire the future development of hyperspectral imaging technology.

NOMENCLATURE

Abbreviations

AOTF	acousto–optic tunable filter
BIL	band interleaved by line
BIP	band interleaved by pixel
BSQ	band sequential
CCD	charge-coupled device
CGH	computer-generated hologram
CMOS	complementary metal-oxide-semiconductor
CTIS	computed tomography imaging spectrometer
CVF	circular variable filter
CW	continuous wave
DASI	digital array scanned interferometer

EMCCD	electron multiplying CCD
FWHM	full width at half maximum
ICCD	intensified CCD
InGaAs	indium gallium arsenide
InSb	indium antimonide
LCTF	liquid crystal tunable filter
LED	light emitting diode
LVF	linear variable filter
MCT	mercury cadmium telluride
MEMS	microelectromechanical systems
NIR	near-infrared
OPD	optical path difference
PbSe	lead selenide
pcLED	phosphor-converted LED
PGP	prism–grating–prism
QE	quantum efficiency
QTH	quartz–tungsten–halogen
RF	radio frequency
ROI	region of interest
SNR	signal-to-noise ratio
UV	ultraviolet
VHIS	volume holographic imaging spectrometer
VIS	visible

REFERENCES

Abbaspour-Tamijani, A., Dussopt, L., & Rebeiz, G. M. (2003). Miniature and tunable filters using MEMS capacitors. *IEEE Transactions on Microwave Theory and Techniques, 51*(7), 1878–1885.

Andor. (2006). *Scientific Digital Camera Solutions: 2006 Catalog*. South Windsor, CT, USA: Andor Technology PLC.

Ariana, D. P., & Lu, R. (2008). Detection of internal defect in pickling cucumbers using hyperspectral transmittance imaging. *Transactions of the ASABE, 51*(2), 705–713.

Bannon, D., & Thomas, R. (2005). Harsh environments dictate design of imaging spectrometer. *Laser Focus World, 41*(8), 93–95.

Bodkin, A. (2007). Hyperspectral imaging at the speed of light. SPIE Newsroom, December 11, 2007; doi: 10.1117/2.1200712.0845.

Bodkin, A., Sheinis, A. I., & Norton, A. (2008). Hyperspectral imaging systems. *US Patent Application Publication*. Pub. No.: US 2008/0088840 A1.

Brauns, E. B., & Dyer, R. B. (2006). Fourier transform hyperspectral visible imaging and the nondestructive analysis of potentially fraudulent documents. *Applied Spectroscopy, 60*(8), 833–840.

Burger, J., & Geladi, P. (2005). Hyperspectral NIR image regression. Part I: Calibration and correction. *Journal of Chemometrics, 19*(5), 355–363.

Chao, K., Mehl, P. M., & Chen, Y. R. (2002). Use of hyper- and multi-spectral imaging for detection of chicken skin tumors. *Applied Engineering in Agriculture, 18*(1), 113–119.

Chao, K., Yang, C. C., Chen, Y. R., Kim, M. S., & Chan, D. E. (2007). Fast line-scan imaging system for broiler carcass inspection. *Sensing and Instrumentation for Food Quality and Safety, 1*(2), 62–71.

Descour, M. R., & Dereniak, E. L. (1995). Computed-tomography imaging spectrometer—experimental calibration and reconstruction results. *Applied Optics, 34*(22), 4817–4826.

Descour, M. R., Volin, C. E., Dereniak, E. L., Gleeson, T. M., Hopkins, M. F., Wilson, D. W., & Maker, P. D. (1997). Demonstration of a computed-tomography imaging spectrometer using a computer-generated hologram disperser. *Applied Optics, 36*(16), 3694–3698.

Goldsmith, C. L., Malczewski, A., Yao, Z. J., Chen, S., Ehmke, J., & Hinzel, D. H. (1999). RF MEMs variable capacitors for tunable filters. *International Journal of RF and Microwave Computer-Aided Engineering, 9*(4), 362–374.

Gómez-Sanchis, J., Gómez-Chova, L., Aleixos, N., Camps-Valls, G., Montesinos-Herrero, C., Moltó, E., & Blasco, J. (2008a). Hyperspectral system for early detection of rottenness caused by *Penicillium digitatum* in mandarins. *Journal of Food Engineering, 89*(1), 80–86.

Gómez-Sanchis, J., Moltó, E., Camps-Valls, G., Gómez-Chova, L., Aleixos, N., & Blasco, J. (2008b). Automatic correction of the effects of the light source on spherical objects: an application to the analysis of hyperspectral images of citrus fruits. *Journal of Food Engineering, 85*(2), 191–200.

Hanley, Q. S., Verveer, P. J., & Jovin, T. M. (1999). Spectral imaging in a programmable array microscope by hadamard transform fluorescence spectroscopy. *Applied Spectroscopy, 53*(1), 1–10.

Hariharan, P. (2007). *Basics of interferometry* (2nd ed., pp. 13–22). San Diego, CA: Elsevier.

Inoue, Y., & Penuelas, J. (2001). An AOTF-based hyperspectral imaging system for field use in ecophysiological and agricultural applications. *International Journal of Remote Sensing, 22*(18), 3883–3888.

Jestel, N. L., Shaver, J. M., & Morris, M. D. (1998). Hyperspectral Raman line imaging of an aluminosilicate glass. *Applied Spectroscopy, 52*(1), 64–69.

Kim, M. S., Chen, Y. R., Cho, B. K., Chao, K., Yang, C. C., Lefcourt, A. M., & Chan, D. (2007). Hyperspectral reflectance and fluorescence line-scan imaging for online defect and fecal contamination inspection of apples. *Sensing and Instrumentation for Food Quality and Safety, 1*(3), 151–159.

Kim, M. S., Chen, Y. R., & Mehl, P. M. (2001). Hyperspectral reflectance and fluorescence imaging system for food quality and safety. *Transactions of the ASAE, 44*(3), 721–729.

Kim, M. S., Lefcourt, A. M., & Chen, Y. R. (2003). Multispectral laser-induced fluorescence imaging system for large biological samples. *Applied Optics, 42*(19), 3927–3934.

Klein, M. E., Aalderink, B. J., Padoan, R., de Bruin, G., & Steemers, T. A. G. (2008). Quantitative hyperspectral reflectance imaging. *Sensors, 8*(9), 5576–5618.

Lawrence, K. C., Park, B., Heitschmidt, G. W., Windham, W. R., & Thai, C. N. (2007). Evaluation of LED and tungsten–halogen lighting for fecal contaminant detection. *Applied Engineering in Agriculture, 23*(6), 811–818.

Lawrence, K. C., Park, B., Windham, W. R., & Mao, C. (2003). Calibration of a pushbroom hyperspectral imaging system for agricultural inspection. *Transactions of the ASAE, 46*(2), 513–521.

Lawrence, K. C., Yoon, S. C., Heitschmidt, G. W., Jones, D. R., & Park, B. (2008). Imaging system with modified-pressure chamber for crack detection in shell eggs. *Sensing and Instrumentation for Food Quality and Safety, 2*(3), 116–122.

Litwiller, D. (2005). CMOS vs. CCD: Maturing technologies, maturing markets. *Photonics Spectra, 39*(8), 54–58.

Liu, W., Barbastathis, G., & Psaltis, D. (2004). Volume holographic hyperspectral imaging. *Applied Optics, 43*(18), 3581–3599.

Lu, R. (2003). Detection of bruises on apples using near-infrared hyperspectral imaging. *Transactions of the ASAE, 46*(2), 523–530.

Lu, R., & Chen, Y. R. (1998). Hyperspectral imaging for safety inspection of food and agricultural products. In Pathogen Detection and Remediation for Safe Eating. *Proceedings of SPIE, Vol. 3544*, 121–133.

Malik, Z., Cabib, D., Buckwald, R. A., Talmi, A., Garini, Y., & Lipson, S. G. (1996). Fourier transform multipixel spectroscopy for quantitative cytology. *Journal of Microscopy, 182*(2), 133–140.

Marinelli, W. J., Gittins, C. M., Gelb, A. H., & Green, B. D. (1999). Tunable Fabry–Perot etalon-based long-wavelength infrared imaging spectroradiometer. *Applied Optics, 38*(12), 2594–2604.

Mergenthaler-Gatfield, S., Holzgreve, W., & Hahn, S. (2008). Spectral karyotyping (SKY): Applications in prenatal diagnostics. In S. Hahn, & L. G. Jackson (Eds.), *Prenatal diagnosis: methods in molecular biology, vol. 444* (pp. 3–26). Totowa, NJ: Humana Press Inc.

Min, M., Lee, W. S., Burks, T. F., Jordan, J. D., Schumann, A. W., Schueller, J. K., & Xie, H. K. (2008). Design of a hyperspectral nitrogen sensing system for orange leaves. *Computers and Electronics in Agriculture, 63*(2), 215–226.

Morris, H. R., Hoyt, C. C., & Treado, P. J. (1994). Imaging spectrometers for fluorescence and Raman microscopy: acousto–optic and liquid-crystal tunable filters. *Applied Spectroscopy, 48*(7), 857–866.

Mueller-Mach, R., Mueller, G. O., Krames, M. R., & Trottier, T. (2002). High-power phosphor-converted light-emitting diodes based on III-nitrides. *IEEE Journal of Selected Topics in Quantum Electronics, 8*(2), 339–345.

Muthu, S., Schuurmans, F. J. P., & Pashley, M. D. (2002). Red, green, and blue LEDs for white light illumination. *IEEE Journal of Selected Topics in Quantum Electronics, 8*(2), 333–338.

Nicolai, B. M., Lotze, E., Peirs, A., Scheerlinck, N., & Theron, K. I. (2006). Non-destructive measurement of bitter pit in apple fruit using NIR hyperspectral imaging. *Postharvest Biology and Technology, 40*(1), 1–6.

Noh, H. K., & Lu, R. (2007). Hyperspectral laser-induced fluorescence imaging for assessing apple fruit quality. *Postharvest Biology and Technology, 43*(2), 193–201.

Okamoto, T., & Yamaguchi, I. (1991). Simultaneous acquisition of spectral image-information. *Optics Letters, 16*(16), 1277–1279.

Orenstein, A., Kostenich, G., Rothmann, C., Barshack, I., & Malik, Z. (1998). Imaging of human skin lesions using multipixel Fourier transform spectroscopy. *Lasers in Medical Science, 13*(2), 112–118.

Palmer, C. (2005). *Diffraction grating handbook* (6th ed., pp. 14–42). Rochester, NY: Newport Corporation.

Park, B., Lawrence, K. C., Windham, W. R., & Buhr, R. J. (2002). Hyperspectral imaging for detecting fecal and ingesta contaminants on poultry carcasses. *Transactions of the ASAE, 45*(6), 2017–2026.

Peng, Y., & Lu, R. (2006). An LCTF-based multispectral imaging system for estimation of apple fruit firmness. Part I: Acquisition and characterization of scattering images. *Transactions of the ASAE, 49*(1), 259–267.

Pham, T. H., Bevilacqua, F., Spott, T., Dam, J. S., Tromberg, B. J., & Andersson-Engels, S. (2000). Quantifying the absorption and reduced scattering coefficients of tissuelike turbid media over a broad spectral range with noncontact Fourier-transform hyperspectral imaging. *Applied Optics, 39*(34), 6487–6497.

Polder, G., van der Heijden, G. W. A. M., Keizer, L. C. P., & Young, I. T. (2003). Calibration and characterisation of imaging spectrographs. *Journal of Near Infrared Spectroscopy, 11*(3), 193–210.

Qin, J., Burks, T. F., Kim, M. S., Chao, K., & Ritenour, M. A. (2008). Citrus canker detection using hyperspectral reflectance imaging and PCA-based image classification method. *Sensing and Instrumentation for Food Quality and Safety, 2*(3), 168–177.

Qin, J., & Lu, R. (2005). Detection of pits in tart cherries by hyperspectral transmission imaging. *Transactions of the ASAE, 48*(5), 1963–1970.

Qin, J., & Lu, R. (2007). Measurement of the absorption and scattering properties of turbid liquid foods using hyperspectral imaging. *Applied Spectroscopy, 61*(4), 388–396.

Qin, J., & Lu, R. (2008). Measurement of the optical properties of fruits and vegetables using spatially resolved hyperspectral diffuse reflectance imaging technique. *Postharvest Biology and Technology, 49*(3), 355–365.

Safren, O., Alchanatis, V., Ostrovsky, V., & Levi, O. (2007). Detection of green apples in hyperspectral images of apple-tree foliage using machine vision. *Transactions of the ASABE, 50*(6), 2303–2313.

Sensors Unlimited. (2006). *What is InGaAs?* Princeton, NJ: Sensors Unlimited, Inc. Application Note.

Smith, W. H., & Hammer, P. D. (1996). Digital array scanned interferometer: Sensors and results. *Applied Optics, 35*(16), 2902–2909.

Spectral Imaging. (2003). *ImSpector imaging spectrograph user manual* Ver. 2.21. Oulu, Finland: Spectral Imaging, Ltd.

Steigerwald, D. A., Bhat, J. C., Collins, D., Fletcher, R. M., Holcomb, M. O., Ludowise, M. J., & Rudaz, S. L. (2002). Illumination with solid state lighting technology. *IEEE Journal of Selected Topics in Quantum Electronics, 8*(2), 310–320.

Wabuyele, M. B., Yan, F., Griffin, G. D., & Vo-Dinh, T. (2005). Hyperspectral surface-enhanced Raman imaging of labeled silver nanoparticles in single cells. *Review of Scientific Instruments, 76*(6), 063710.

Yoon, S. C., Lawrence, K. C., Smith, D. P., Park, B., & Windham, W. R. (2008). Bone fragment detection in chicken breast fillets using transmittance image enhancement. *Transactions of the ASABE, 51*(1), 331–339.

Zhang, H., Paliwal, J., Jayas, D. S., & White, N. D. G. (2007). Classification of fungal infected wheat kernels using near-infrared reflectance hyperspectral imaging and support vector machine. *Transactions of the ASABE, 50*(5), 1779–1785.